JOC The Journal of Organic Chemistry

Featured Article

pubs.acs.org/joc

Small-Molecule Fluorophores with Large Stokes Shifts: 9-Iminopyronin Analogues as Clickable Tags

Peter Horváth, Peter Šebej, Tomáš Šolomek, and Petr Klán*

Department of Chemistry and RECETOX, Faculty of Science, Masaryk University, Kamenice 5, 625 00 Brno, Czech Republic

Supporting Information

ABSTRACT: The design, synthesis, and both experimental and theoretical studies of several novel 9-(acylimino)- and 9-(sulfonylimino)pyronin derivatives containing either an oxygen or a silicon atom at position 10 are reported. These compounds, especially the Si analogues, exhibit remarkably large Stokes shifts (around 200 nm) while still possessing a high fluorophore brightness, absorption bands in the near-UV and visible part of the spectrum, and high thermal and photochemical stabilities in protic solvents. The reason for the observed large Stokes shifts is an intramolecular charge-transfer excitation of an electron from the HOMO to the LUMO of the chromophore, accompanied by elongation of the C9−N bond and considerable solvent reorganization due to hydrogen bonding to the solvent. Due to the photophysical properties of the studied compounds and their facile and high-yielding synthesis, as well as a simple protocol for their bioorthogonal ligation to a model saccharide using a Huisgen alkyne−azide cycloaddition, they represent excellent candidates for biochemical and biological applications as fluorescent tags and indicators for multichannel imaging. 9-(Acylimino)pyronins alter their optical properties upon protonation and may also be used as pH sensors.

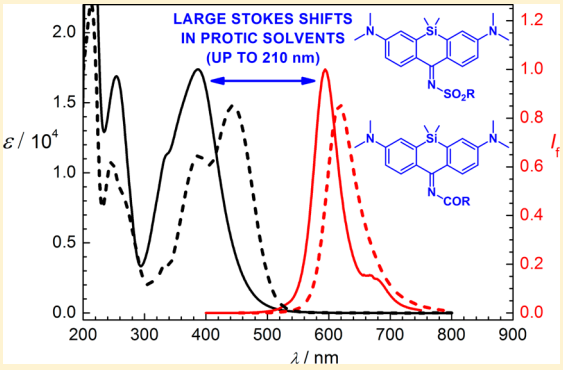

INTRODUCTION

Small-molecule organic fluorophores with tailored chemical and photophysical properties have become an essential tool for imaging and sensing in biochemistry, biophysics, molecular biology, medicine, and material sciences.[1−5] The major benefit of utilizing synthetic fluorophores is the opportunity to carefully design their chemical and spectroscopic properties using methods of modern organic chemistry.[1,5] Various bioconjugation strategies that involve fluorescent dye markers have also been developed.[6]

Newly designed fluorophores for bioapplications should be thermally and photochemically stable, nontoxic, sufficiently soluble in water, absorb visible light with large molar absorption coefficients, and emit light efficiently in the red or near-infrared parts of the spectrum, where a higher signal-to-noise ratio due to low background autofluorescence and enhanced tissue penetration (650−950 nm)[7,8] are of a great benefit. High fluorophore brightness, proportional to the product of the decadic molar absorption coefficient and the fluorescence quantum yield, allows visualization at low fluorophore concentrations, which suppresses their aggregation and improves optical resolution in single-molecule microscopy.[9] Aggregation of fluorophores in solutions may result in self-quenching and loss of fluorescence intensity.

Self-quenching occurs principally in fluorophores with small Stokes shifts.[9] Therefore, a large Stokes shift is a very important attribute of a fluorophore. In addition, a cleverly designed set of fluorophores with large Stokes shifts can enable multichannel imaging.[10] Large Stokes shifts are common for fluorescent proteins,[11] metal complexes,[12,13] quantum dots,[14] or UV absorbing chromophores. However, these fluorophore families lack one or more of the advantages that are connected to the small-molecule organic fluorophores mentioned above.

Excited-state geometry relaxation accompanied by solvent reorganization are required to achieve a substantial Stokes shift.[15] This usually leads the molecule to explore a considerable part of its excited state potential energy surface where conical intersections can be encountered, and as a result, the excited state can be deactivated via a radiationless internal conversion decreasing the fluorescence quantum yield.[16] Rotation of a π-conjugated substituent in the molecular structure of a fluorophore has been proposed to yield a large Stokes shift,[17] but it is rather difficult to predict the nature and the position of such substituents in a fluorophore, because detailed guidelines, though under development,[18] are still incomplete. Other strategies based on Förster resonance energy transfer (FRET) do not entirely eliminate the self-quenching and inner-filter effects.[19]

In this report, we describe the design, synthesis, and photophysical properties of novel 9-(acylimino)- and 9-(sulfonylimino)pyronin fluorophores containing oxygen and silicon at position 10 that exhibit remarkably large Stokes shifts, a high fluorophore brightness, and high thermal and photo-

Received: September 26, 2014
Published: December 8, 2014

   dx.doi.org/10.1021/jo502213t | J. Org. Chem. 2015, 80, 1299−1311

chemical stability. An explanation for the observed Stokes shifts is suggested and corroborated by quantum chemical calculations. The effects of the structure modifications as well as of solution pH are discussed. We also demonstrate that a facile ligation strategy can be used to attach the 9-iminopyronin fluorophores to a model saccharide.

RESULTS

Synthesis of 1 and 2. The synthesis of the target 9*H*-xanthene-3,6-diamine derivatives, **1a,b**, and their analogues containing silicon at position 10, **2a,b**, is depicted in Scheme 1.

Scheme 1. Synthesis of 1a,b and 2a−e

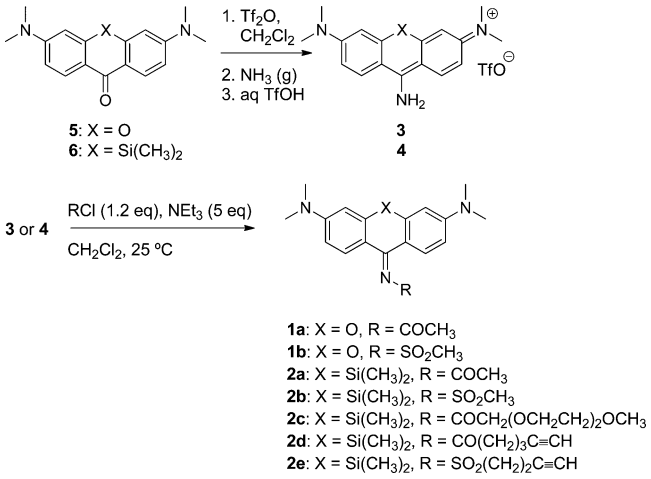

In the first step, 9-aminopyronin **3** and silicon-containing 9-aminopyronin **4** were prepared from the xanthenone analogues **5** and **6** in very good yields (85−97%) according to a procedure adopted from Wu and Burgess.[20] The isolated 9-aminopyronins were subsequently converted to the title 9-imino derivatives **1a,b** and **2a,b** by a reaction with acyl or sulfonyl chlorides in 74−92% yields. The overall yields over the two steps were 63−90%. A more water-soluble derivative **2c** was also prepared.

The alkynyl derivatives **2d** and **2e** synthesized in the same way from **4** (Scheme 1) in 89 and 38% yield, respectively, were linked to 2-azido-2-deoxy-D-glucose using a copper(I)-catalyzed azide−alkyne cycloaddition reaction[21] in excellent yields (90 and 86%, respectively; Scheme 2). The resulting 1,2,3-triazoles **2f,g** were mixtures of two regioisomers in an approximately 55:45 ratio (see the Experimental Section for further details).

Photophysical Properties in Methanol and Aprotic Solvents. The absorption spectra of the O- and Si-atom containing 9-(acylimino)-9*H*-xanthene-3,6-diamines (or 9-(acylimino)pyronins) **1a**, **2a**, **2c**, **2d**, and **2f** in methanol possessed a major absorption band at λ_{abs}^{max} = 375−400 nm (Table 1; **2a**: Figure 1), the position of which was insignificantly affected by polar or protic properties of a solvent (the absorption spectra of **2a** in CH_2Cl_2, CH_3CN, DMSO, and methanol are shown in Figure S39, Supporting Information). These compounds showed bright fluorescence at room temperature with the quantum yields of Φ_f from 0.28 to 0.56 in methanol but were barely or nonemissive in aprotic solvents. In addition, Figure S40 shows the changes in the fluorescent spectra of **2a** in acetonitrile upon addition of small amounts of methanol; the emission intensity increased significantly, and λ_{em}^{max} was shifted bathochromically by about 30 nm. The emission band maxima of the Si-analogues **2a,c,d,f** (λ_{em}^{max} ∼600 nm) were shifted bathochromically relative to the oxygen analogue **1a** (λ_{em}^{max} ∼510 nm). The corresponding Stokes shifts were ∼200 nm (∼9090 cm^{-1}) for Si-analogues and 137 nm (7100 cm^{-1}) for the O-analogue **1a**.

Scheme 2. Copper(I)-Catalyzed Alkyne−azide Cycloaddition of 2c,d with 2-Azido-2-deoxy-D-glucose To Give 2f,g (Only One Regioisomer Is Shown for Clarity)

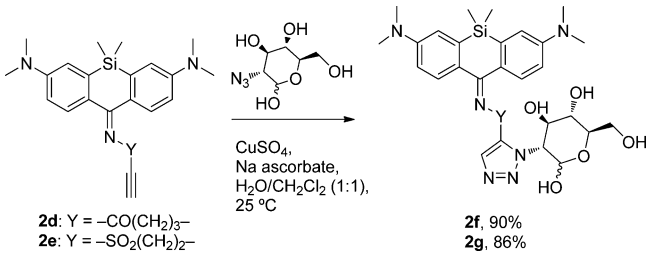

The absorption and emission bands of the 9-(alkylsulfonyl)-iminopyronins **1b**, **2b**, **2e**, and **2g** were bathochromically shifted (λ_{abs}^{max} = 422−452 nm; λ_{em}^{max} = 525−617) compared to those of the 9-(acylimino) derivatives (Table 1; Figure 1 and Figure S48, Supporting Information), and the effect of the atom at position 10 was analogous to that observed in the acyl series. The fluorescence quantum yields (Φ_f = 0.23−0.43) and the Stokes shifts (103−173 nm) were slightly smaller than those of 9-(acylimino)pyronins. The spectroscopic properties of the xanthenones **5** and **6**, also studied elsewhere,[22] are shown in Table 1 for comparison. The fluorescence decay of **2f** and **2g** (Table 1) obeyed a single-exponential rate law with a lifetime similar to that of fluorescein[23] (τ = 4.0 ns).

Photophysical Properties in Aqueous Solutions. We evaluated the acid−base properties of **2** in aqueous solutions. In general, both λ_{abs}^{max} and λ_{em}^{max} were only slightly bathochromically shifted compared to those observed in methanol. The acid dissociation constants of the water-soluble 9-(acylimino)-Si-pyronin (**2c**) and 9-(sulfonylimino)-Si-pyronin (**2b**) derivatives were obtained by spectrophotometric titration of their aqueous solutions with 1% of DMSO as cosolvent. A series of UV−vis spectra was measured by addition of 0.01 mol dm^{-3} HCl to a solution of **2c** or **2b** in 0.01 mol dm^{-3} aqueous NaOH or 0.01 mol dm^{-3} NaOH to a solution of **2c** or **2b** in 0.01 mol dm^{-3} aqueous HCl. The acid dissociation constants (ionization quotients at ionic strength I = 0.1 mol dm^{-3}) resulting from a global analysis of the spectra and fitting of a titration function provided the pK_as of 6.77 ± 0.06 for **2c** and approximately 2−3 for **2b** (Table 2; see Figure S62 for details). The global analyses provided the species spectra identical to those determined spectrophotometrically (Table 2, Figure 2).

The absorption and emission spectra of the 9-(acylimino) derivative **2f** measured at low and high pH values are shown in Figures 2a,b, and the corresponding photophysical parameters are listed in Table 2. The spectra obtained under physiological conditions (PBS, pH = 7.4) are portrayed in the same figure for comparison (Figure 2c). The λ_{abs}^{max} (401 nm) and λ_{em}^{max} (606 nm) values as well as the Stokes shifts determined at pH above the corresponding pK_a (Figure 2a; pK_a = 6.76 ± 0.11) were similar to those obtained in methanol (for example, **2f**: λ_{abs}^{max} = 386 nm and λ_{em}^{max} = 596 nm; Table 1, Figure S61), and this species is assigned to the neutral base B (Scheme 3). The spectrum observed at low pH was assigned to the acid A. In this case, the absorption maxima are substantially bathochromically shifted (λ_{abs}^{max} (**2f**) = 664 nm), whereas the emission maxima are shifted only slightly compared to those of the base B. The corresponding Stokes shifts

dx.doi.org/10.1021/jo502213t | J. Org. Chem. 2015, 80, 1299−1311

Table 1. Spectroscopic Properties of 1, 2, 5, and 6 in Methanol

compd	λ_{abs}^{max} (nm)	log ε (dm^3 mol^{-1} cm^{-1})	λ_{em}^{max} (nm)	Φ_f (τ/ns[a])	Stokes shift (nm) (cm^{-1})	$\varepsilon\Phi/10^3$ (dm^3 mol^{-1} cm^{-1})[b]
5	379	4.63	442	0.56 ± 0.03	63 (3760)	23.9
1a	376	4.32	513	0.36 ± 0.01	137 (7100)	7.5
1b	422	4.19	525	0.33 ± 0.02	103 (4650)	5.1
6	402	4.51	489	0.40 ± 0.03	87 (4430)	12.9
2a	387	4.24	597	0.56 ± 0.04	210 (9090)	9.7
2c	400	4.21	596	0.47 ± 0.04	196 (8220)	7.6
2d	387	4.40	595	0.28 ± 0.03	208 (9030)	7.0
2f	386	4.34	596	0.30 ± 0.03 (2.31 ± 0.01)	208 (9130)	6.6
2b	444	4.17	617	0.23 ± 0.01	173 (6370)	3.4
2e	452	4.30	617	0.43 ± 0.02	165 (5920)	8.6
2g	448	4.18	616	0.36 ± 0.03 (3.06 ± 0.01)	168 (6090)	5.4

[a]Fluorescence lifetimes (τ). [b]Brightness of the fluorophore (the product of the molar absorption coefficient at λ_{abs}^{max} and the corresponding fluorescence quantum yield).

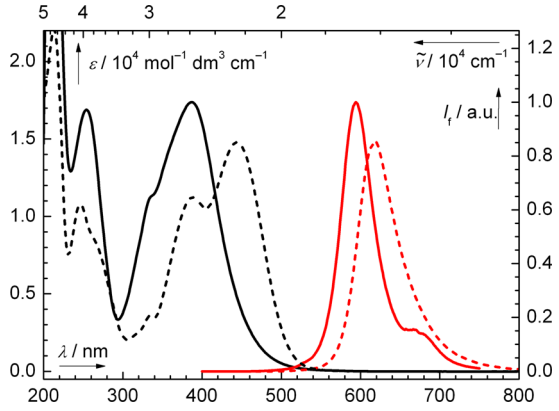

Figure 1. Absorption (black line) and normalized emission (red line) spectra of **2a** (solid lines; $c = 7.4 \times 10^{-5}$ mol dm^{-3}; $\lambda_{exc} = 389$ nm) and **2b** (dashed lines; $c = 6.2 \times 10^{-5}$ mol dm^{-3}; $\lambda_{exc} = 443$ nm) in methanol.

are relatively small (below 20 nm). Under physiological conditions (PBS, pH = 7.4), the spectra revealed the presence of both acid–base forms (Figure 2c) and are equal to those observed under the extreme pH conditions. In addition, nearly identical spectroscopic behavior was observed for **2c** (Table 2). The analysis of series of ^{1}H NMR spectra of **2a** (in a buffered CD_3OD/D_2O (4:1, v/v) solution) exhibited a similar change of the spectral properties and allowed us to estimate the p$K_a \sim 6$ (Figure S31). The exchange of the acidic proton (form A) is fast enough to show only an average NMR signals instead of signals of two species. The pK_a of the 9-(alkylsulfonyl)imino derivative **2g** could not be determined accurately because the compound is hydrolyzed at pH below 3 in the dark within minutes. However, the estimated value of p$K_a \sim 2$–3 ensures that only the base B is present at pH = 7.4 (Figure 3). The fluorescence quantum yields and fluorescence lifetimes for **2f,g** (Table 2) in a PBS buffer are similar to those determined in methanol.

A possible excited-state proton-transfer (ESPT)[9] process was investigated for **2g** by measuring the absorption and fluorescence spectra as a function of the acetate buffer concentration (Figure S69). The pH of the solution was kept at ~4.6, i.e., higher than the corresponding pK_a value (~2–3; Table 2). The absorption spectrum of **2g** was not affected by the buffer concentration in the range of 0.03 and 3 M. However, while only one emission band ($\lambda_{em}^{max} = 629$ nm) dominated the spectrum at a low buffer concentration, a new band at $\lambda_{em}^{max} = 693$ nm appeared as a major emission peak at a very high buffer concentration.

No change of the absorption spectra, usually associated with dye aggregation in polar media,[24,25] was observed in the case of **2f** and **2g** in PBS/DMSO (99:1, v/v) in the concentration range

Table 2. Spectroscopic Properties of 2 in Aqueous Solutions

compd	pK_a[a]	pH[b]	λ_{abs}^{max} (nm)	log ε (dm^3 mol^{-1} cm^{-1})	λ_{em}^{max} (nm)	Φ_f (τ/ns[f])	Stokes shift (nm) (cm^{-1})	$\varepsilon\Phi/10^3$ (dm^3 mol^{-1} cm^{-1})[e]
2c	6.77 ± 0.06	3.0	666	4.92	681	0.28 ± 0.02 (2.32 ± 0.01)	15 (330)	23.3
		11.0	418	4.11	607	0.46 ± 0.01 (2.34 ± 0.01)	189 (7450)	5.9
2f	6.76 ± 0.11	3.0	664	5.09	682	0.26 ± 0.04 (2.10 ± 0.02)	18 (400)	32.0
		11.0	401	4.25	606	0.35 ± 0.03 (1.90 ± 0.01)	205 (8440)	6.2
2b	2–3	7.4[c]	469	n.d.	630	n.d.	161 (5450)	n.d.
2g	2–3	3.0[d]	667	n.d.	692	n.d.	25 (540)	n.d.
		7.4	469	4.04	631	0.43 ± 0.03 (2.79 ± 0.01)	157 (5470)	4.7

[a]The pK_a values were determined by titration (see the text). The values for **2b,g** could not be determined precisely. [b]$I = 0.1$ mol dm^{-3} adjusted by KCl; 1% of DMSO was added as a cosolvent. pH of the solution was determined using a calibrated glass electrode. [c]10% of DMSO was added as a cosolvent. [d]These values were determined at pH = 3.0 at which the compound is sufficiently stable in the dark; both forms A and B (Scheme 3) were present; an estimated amount of the form B was <20%. [e]See footnote b in Table 1. [f]See footnote a in Table 1.

dx.doi.org/10.1021/jo502213t | J. Org. Chem. 2015, 80, 1299–1311

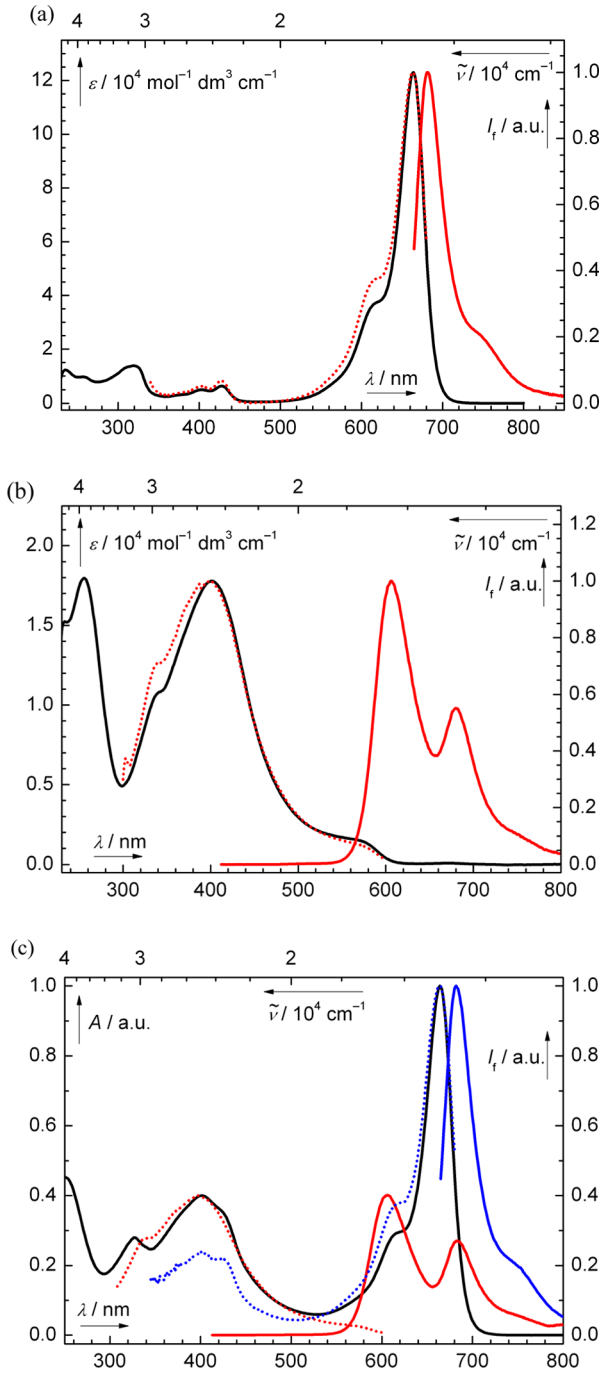

Figure 2. (a) Absorption (black solid line; $c = 1.9 \times 10^{-5}$ mol dm^{-3}), normalized emission (λ_{exc} = 664 nm; red solid line), and normalized excitation (λ_{em} = 682 nm; red dotted line) spectra of **2f** in aqueous HCl/DMSO (99:1, v/v; I = 0.1 mol dm^{-3}, KCl) at pH = 3.0. (b) Absorption (black solid line; $c = 1.6 \times 10^{-5}$ mol dm^{-3}), normalized emission (λ_{exc} = 401 nm; red solid line), and normalized excitation (λ_{em} = 606 nm; red dotted line) spectra of **2f** in aqueous KOH/DMSO (99:1, v/v; I = 0.1 mol dm^{-3}, KCl) at pH = 11.0. (c) Absorption (black solid line, $c \sim 1.1 \times 10^{-5}$ mol dm^{-3}), normalized emission (λ_{exc} = 401 nm; red solid line; λ_{exc} = 664 nm; blue solid line) and normalized excitation (λ_{em} = 606 nm; red dotted line; λ_{em} = 682 nm; blue dotted line) spectra of **2f** in PBS/DMSO (99:1, v/v) at pH = 7.4.

from 9×10^{-8} to 3×10^{-4} mol dm^{-3} (Figures S64 and S68). The upper concentration value represents the limit of the solubility of the dye in an aqueous solution (I = 0.1 mol dm^{-3}).

Scheme 3. Acid–base Equilibrium for 1 and 2

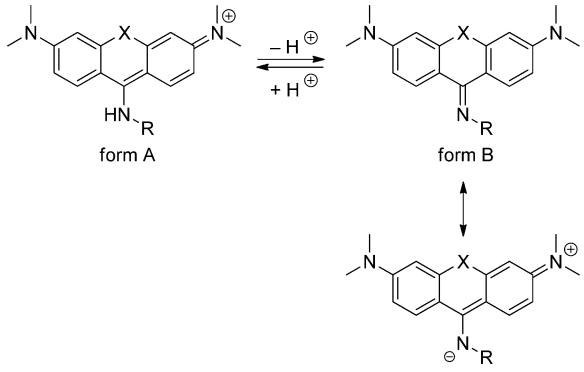

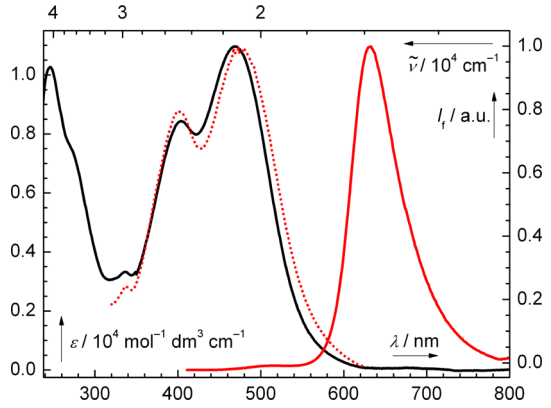

Figure 3. Absorption (black solid line; $c = 2.7 \times 10^{-5}$ mol dm^{-3}), normalized emission (red solid line, λ_{exc} = 401 nm), and normalized excitation (λ_{em} = 632 nm; red dotted line) spectra of **2g** in PBS/DMSO (99:1, v/v) at pH = 7.4.

Chemical Stability. The chemical stability of **2f**,**g** in the dark was determined in various solvents (methanol, DMSO and PBS/DMSO, 99:1, v/v). A plot of the dye absorbance λ_{abs}^{max} against time was used to calculate the half-lives of the compounds by fitting the data with a pseudo-first order kinetic equation. The decomposition half-lives of **2f** were $\tau_{1/2}$ = 33 h^{-1} and $\tau_{1/2} > 10^4$ h^{-1} in PBS/DMSO and DMSO, respectively, at 20 °C. Compound **2g** was even more stable ($\tau_{1/2}$ = 750 h^{-1} in PBS/DMSO; for details see the Supporting Information, page S2). The compounds **2f** (Figure 4) and **2a** (Figure S38) exhibited a full reversibility between the acid A and base B forms over five cycles of periodic addition of aq HCl and NaOH between pH 3.0 and 11.0.

Both **2f** and **2g** decomposed in methanol and PBS/DMSO upon irradiation using 32 high-energy LEDs (λ_{em} = 470 nm, Figure S71) or a diode-laser (λ_{em} = 375 nm, Figure S70). The decomposition was about 4-fold faster in aqueous solutions than that in methanol with the half-life of ∼1 h for **2g** in PBS solution (Supporting Information).

Quantum-Chemical Calculations. We performed a conformational analysis of the studied dyes **1a**,**b** and **2a**,**b** in their ground electronic states. Two distinct conformations were identified for each compound (Figure S72 and Table S4), and the geometries of those with the lowest potential energies were then chosen to represent the Franck–Condon points from which the excited-state geometry optimizations started. The absorption maxima of the pairs of conformers did not differ by more than 10 nm. Inspection of the optimized geometries revealed that the bond between a C9 substituent and the C9 carbon atom (C9–N

dx.doi.org/10.1021/jo502213t | J. Org. Chem. 2015, 80, 1299–1311

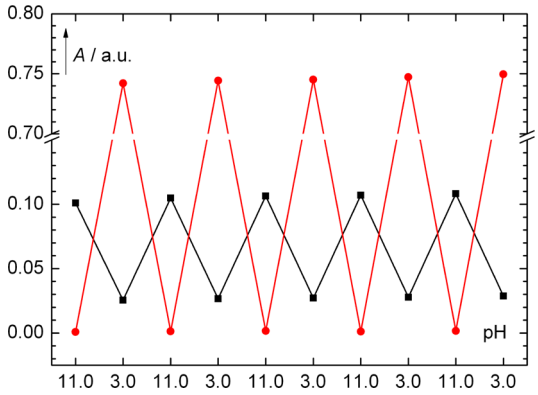

Figure 4. Changes of absorbance (at λ_{obs} = 401 nm; black full square and λ_{obs} = 664 nm; red full circle) of **2f** ($c = 6 \times 10^{-6}$ mol dm^{-3}) upon repeating changes of pH (pH = 11.0, aq NaOH; pH = 3.0, aq HCl) in an aq 0.1 mol dm^{-3} KCl/DMSO (99:1, v/v) solution. The solid line is shown to guide the eye.

bond length denoted as *j*; Figures S74–S84) has a partial double-bond character.

The lowest energy electronic transition in all studied compounds is well described by a transition of a single electron between the frontier molecular orbitals. The excitation of the B form of **1** and **2** is accompanied by a large charge redistribution and can thus be described as an intramolecular charge-transfer (ICT) transition. However, our gas-phase calculations suggest that a locally excited (LE) state may become the lowest excited state in a nonpolar environment. The LUMO possesses a character of an antibonding orbital of π-symmetry of the C9–N bond (Figure S73). The extent to which the p_z orbital of the C9-nitrogen atom contributes to the LUMO depends strongly on the chemical character and the steric bulk of the whole C9 substituent. The major geometric change upon excitation is associated with the length of the C9–N bond (*j*). The geometry of **2a**, which possesses the largest Stokes shift (in nm) in its ground and first excited electronic states, is shown in Figure 5. The corresponding geometries for **1a**,**b**, **2b**, and **5**–**8** are compared in Figures S72–S81.

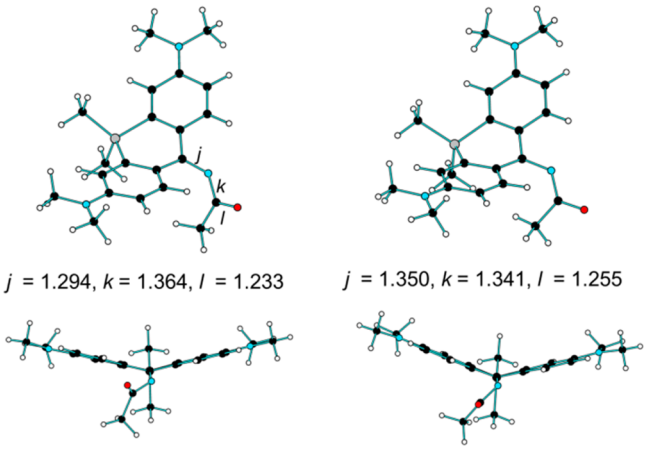

Figure 5. Structure of **2a** (form B) in its ground (left) and first excited electronic state (right) and the corresponding bond lengths (*j*–*l*). A complete picture with all bond lengths can be found in Figure S78 (Supporting Information). The color coding is as follows: C (black), H (white), N (light blue), O (red), and Si (gray).

The computed wavelengths, which correspond to the vertical excitation energies of absorption and fluorescence, and the corresponding Stokes shifts, are compared to the experimental values in Table 3.[26]

Table 3. Comparison of Experimental and Theoretical Absorption and Emission Properties of the Studied Dyes

	experiment[a]			calculations[b]		
compd	λ_{abs}^{max} (nm)	λ_{em}^{max} (nm)	Stokes shift (cm^{-1})	λ_{abs}^{max} (nm)	λ_{em}^{max} (nm)	Stokes shift (cm^{-1})
1a (form A)	549	577	890	473	502	1257
1a (form B)	376	513	7100	414	497	4051
1b	422	525	4650	435	494	2766
2a (form A)	658	678	450	522	542	687
2a (form B)	387	597	9090	436	548	4694
2b	444	617	6370	471	545	2881
3 (form A)	432	478	2230	400	441	2335
3 (form B)	353	482	7580	375	527	7689
5	379	442	3760	388	422	2062
6	402	489	4430	417	458	2163
7a	547[c]	562[c]	490	453	476	1073
7b	499[d]	558[d]	2120	431[e]	468[e]	1822
8	636[f]	648[f]	290	499	519	792

[a]In methanol. [b]See the Experimental Section for details. [c]From Nagano and co-workers.[28] [d]Figure 6; R^3 = diethylamino, R^4 = $-(CH_2)_5-$) in CH_2Cl_2; from Wu and Burgess.[20] [e]In CH_2Cl_2; modeled within the PCM approach [f]From Klán and co-workers.[22]

The vibronic analysis of the absorption and fluorescence spectra of **1** and **2** (forms B) within the Franck–Condon method using the FCclasses program[27] showed that the overlap of the zero-point vibrational wave functions of the ground and the first excited electronic states is very small. Inspection of the Duschinsky matrices revealed that a number of normal modes in the first excited state, that are related to vibrations of the C9-substituent, are expressed by a large number of normal modes of the ground electronic state. On the other hand, the vibronic spectra could be easily obtained for **5** and **6**.

DISCUSSION

The Stokes shifts of the pyronin analogues modified at positions 9 and 10 (Figure 6; e.g., X = O, CR_2, SiR_2; R^3 = aryl, alkyl; R^4 = H, alkyl), in which the first absorption band is described by the HOMO–LUMO electron transition, are typically very small, in the range of 20–30 nm.[28–32] However, shifts of up to ~80 nm for highly fluorescent 9-(alkylamino)- and 9-(dialkylamino)-pyronins (7: X = O; R^3 = dialkylamino; Figure 6) have been reported by Burgess et al.[20,33] A recent patent showed that

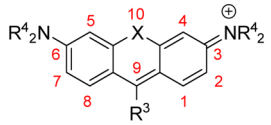

7 a: X = O, R^3 = H, R^4 = CH_3
b: X = O, R^3 = dimethylamino, R^4 = CH_3
8: X = $Si(CH_3)_3$, R^3 = H, R^4 = CH_3

Figure 6. Pyronin derivatives.

dx.doi.org/10.1021/jo502213t | J. Org. Chem. 2015, 80, 1299–1311

further modifications of the 9-(alkylamino)pyronin (**7**: X = O, CR_2, S; Figure 6) aromatic core and the C3- and C6-amino groups may lead to Stokes shifts of up to 180 nm.[34] However, the origin of these large Stokes shifts has not been elucidated. Although only a few pyronin analogues bearing a substituted nitrogen-atom at position 9, such as alkylamino, dialkylamino,[20,35,36] or bis(trimethylsilyl)amino[37] groups, have been reported, 9-(dialkylamino)pyronins have already been used in a recent study of protein−protein interactions.[38] We therefore assumed that pyronins substituted by nitrogen-atom containing substituents at position 9 could be excellent candidates for fluorophores that exhibit very large Stokes shifts.

Wu and Burgess have proposed that an acid−base equilibrium is likely established by treating 9-(alkylamino)pyronin **9** (form A) with triethylamine as a base to form a deprotonated species B (Scheme 4).[20] This form was reported to be nonfluorescent, which is rather unexpected because the ketones **5** and **6** as structural analogues are highly fluorescent (Table 1).

Scheme 4. Acid−Base Equilibrium in 9 Proposed by Wu and Burgess[20]

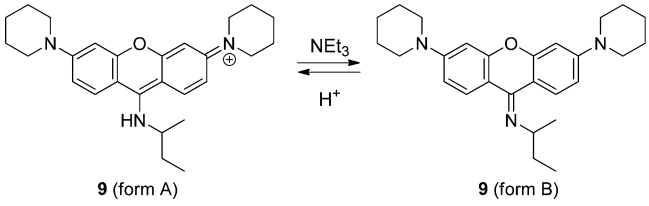

A detailed inspection of the spectral data reported for 9-(alkylamino)pyronins[20] reveals that pyronins with monoalkylamino groups at the position 9 possess slightly larger Stokes shifts than those with dialkylamino groups. Because of the bulkier nature of the secondary amino group, we hypothesized that the *N*-alkyl groups tend to avoid the hydrogen atoms at positions 1 and 8 (Figure 6), thereby decreasing the coplanarity of the chromophore found in the case of a monoalkylamino derivative by single-crystal X-ray analysis.[20] Such an interaction should lead to a decreased overlap of the nitrogen lone electron pair with the molecular orbitals (MOs) of the pyronin chromophore affecting its spectral properties, such as Stokes shifts. The frontier MOs of **3** (forms A and B) and **7b** calculated by DFT are shown in Figure 7 (see also Figure S73 for **5**, **1a**, and **8**). It is obvious that the nodal properties of the frontier orbitals are the same for all the studied compounds but the overlap of the p_z orbital of the C9 nitrogen atom in **7b** with the C9 p_z orbital in the LUMO is smaller than that in **3**, which confirms our hypothesis. A π−bonding interaction increasing the C9−N bond order exists in planar **3**, which is evidenced by a much shorter C9−N bond length than that in **7b** (Figures S82−S84) or than is typical, for example, in anilines (1.355 Å).[39] The antibonding arrangement between the C9 and nitrogen atoms in the LUMO suggests that promotion of an electron from the HOMO to the LUMO upon excitation will elongate the C9−N bond, and can be a reason for the observed large Stokes shifts. Their magnitude will then be closely related to the C9−N bond order and the overlap of the C9 nitrogen p_z orbital in the LUMO. Indeed, a comparison with the spectral properties of the analogous ketones **5** and **6** (Table 1; Figures S73, S80−S81) reveals that their Stokes shifts are substantial, probably as a consequence of an elongation of the C9−O bond.[40] Unfortunately, no additional substituent can be

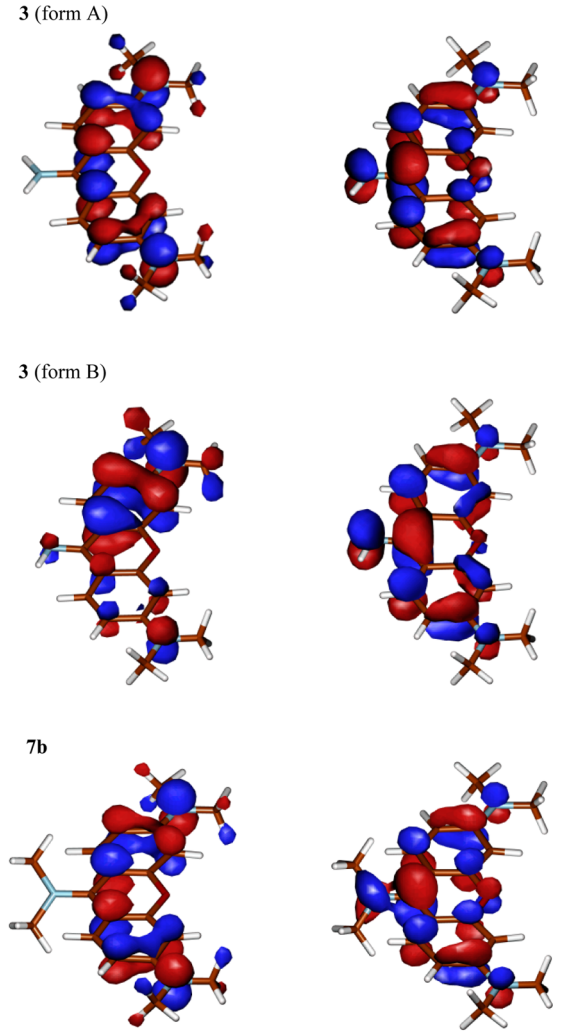

Figure 7. Frontier molecular orbitals (left: HOMO; right: LUMO) of **3** and **7b** computed on the ground-state geometries (see the Experimental Section).

installed on the oxygen atom to tune the dyes' spectral properties and preserving simultaneously the carbonyl character in **5** or **6**.

Once we postulated that increasing the C9−N bond order could lead to elevated Stokes shifts, we advanced to prepare pyronin derivatives possessing a formal double C9−N bond. Because the C9 nitrogen atom in the deprotonated form B must be fairly basic due to a negative charge on nitrogen in one of the mesomeric structures (Scheme 3), its conjugation with an electron-withdrawing group, such as an acetyl and, particularly, a sulfonyl group, was expected to stabilize the imino form B. To date, there is only a single report on the preparation of a 9-sulfonylaminopyronin derivative.[41] In this patent, a base-promoted rearrangement of 9-sulfamoylphenylpyronin in methanol is shown to give 9-alkyl(benzenesulfonyl)-aminopyronin which, nonetheless, cannot attain the imino form B due to the presence of two substituents on the C9-nitrogen atom. 9-Imino-substituted pyronins have thus never been reported before.

For this work, a facile synthesis of Wu and Burgess[20] was modified to provide crystalline, colored 9-imino-O- (**1a**,**b**) and Si-pyronins (**2a**−**e**) (Scheme 1) in high yields. All synthesized pyronins are soluble in polar organic solvents, and the 9-(sulfonylimino)pyronins **1b** and **2b** as well as the 9-(acylimino)-

dx.doi.org/10.1021/jo502213t | J. Org. Chem. 2015, 80, 1299−1311

O-pyronin **1a** are also partially soluble in aqueous solutions. The 9-acylimino-Si-pyronin analogues had to be modified to get a more water-soluble derivative **2c**. Our $^{1}H-^{15}N$ g-HMBC examination confirmed the existence of a formal C9−N double bond in **2** in the solution (Figures S32 and S43). The observed ^{15}N shifts of 321 ppm (**2a**) and 281 ppm (**2b**) are outside the region of chemical shifts typical for an amidic nitrogen (80−170 nm),[42] and can be compared to those of the *N*-acetylacetophenone imines[43] and 3-oxo-5-methylpyrazine derivatives.[44]

All compounds were found to be strongly fluorescent (Φ_f in the range of 0.23−0.56) in protic solvents, apparently contradicting the original observation that **9** (B) is nonfluorescent in dichloromethane.[20] Indeed, only barely detectable or no fluorescence from the compounds **1** and **2** was observed in aprotic solvents (Figure S40). These compounds exhibit remarkably large Stokes shifts (Table 1 and 2): 103−137 nm (4.4−7.1 × 10^3 cm^{-1}) for O-pyronins and particularly 157−210 nm (5.5−9.1 × 10^3 cm^{-1}) for Si-pyronins in methanol as well as aqueous solutions when pH is kept above their pK_a's. The positions of the major absorption and emission bands in **1** and **2** are markedly affected by the substitution at position 10. The replacement of oxygen by silicon caused bathochromic shifts of the band maxima in all solvents, which has also been previously reported for various rhodamine dyes.[28−30] Besides the large Stokes shifts, it should be noticed that the λ_{abs}^{max} and λ_{em}^{max} values of **1** and **2** in protic methanol (Table 1, Figure 8) are similar to those of the ketones **5** and **6**, suggesting that the lowest excited state in both types of chromophores may possess an analogous intramolecular charge-transfer (ICT)[9,45] character. In contrast, the lack of fluorescence in aprotic solvents for **1** and **2** indicates that a locally excited (LE) species without charge separation should be the lowest, nonemissive excited state in the absence of H-bonding stabilization, as was also supported by our gas-phase calculations. Thus, a solvent reorganization must add significantly to the overall Stokes shift. Unlike most cases where a fluorescent compound is weakly fluorescent in protic solvents and strongly fluorescent in aprotic media,[9] this is an unusual behavior, although a few other examples can also be found in the literature.[46,47] Our observation of a substantial increase in the fluorescence intensity from **2a** in acetonitrile upon addition of a small amount of methanol (while keeping the solvent polarity as low as possible at very low methanol concentrations) without observing any pronounced bathochromic shift of λ_{em}^{max} (Figure S40) supports our presumption that the appearance of the emission peak is due to H-bonding stabilization[48] of an ICT state at the expense of an LE state.

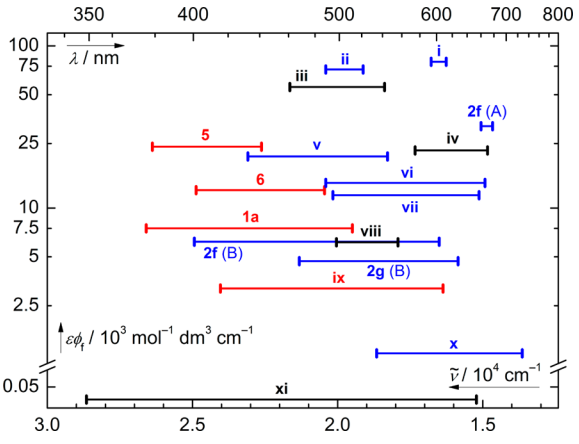

Figure 8. Comparison of the optical properties of known monochromophoric transition-metal-free small-organic molecule fluorophores and several common dyes with those of 9-iminopyronins. The absorption (λ_{abs}^{max} or $\tilde{\nu}_{abs}^{max}$) and emission (λ_{em}^{max} or $\tilde{\nu}_{em}^{max}$) maxima (as the ends of the abscissas), the fluorophore brightness, and solvents in which the data were measured (blue: aqueous solution; red: methanol or ethanol (only for **ix**); black: aprotic organic solvents; CH_2Cl_2 (**iii**, **viii**), $CHCl_3$ (**iv**), THF(**xi**)) are shown. The fluorophores: sulforhodamine 101 (**i**),[56] fluorescein (**ii**),[58,59] a 9-alkylaminopyronin derivative (**iii**),[20] a perylene derivative (**iv**),[62] ATTO 430LS (**v**),[61] a 9-(alkylamino)pyronin analogue, AZ 312 (**vi**),[34] ATTO 490LS (**vii**),[61] a 9-dialkylaminopyronin derivative (**viii**),[20] a 4-trifluoromethyl-7-aminocoumarin derivative (**ix**),[63] a naphthofluorescein derivative (**x**),[64] and a 2,5-bis(2-thienyl)pyrrole derivative (**xi**).[60] The values of Stokes shifts for the compounds studied in this work (depicted by Arabic numerals) are shown in Tables 1−3; the Stokes shifts of the common dyes (depicted by Roman numerals, **i**−**iv**, **vi**, and **viii**−**xi**) and their structures are provided in Figure S1 and Table S3 (Supporting Information).

For this work, we also investigated whether the fluorophores undergo an intermolecular excited-state proton transfer (ESPT) by measuring the absorption and fluorescence spectra as a function of the acetate buffer concentration, analogous to the studies of ESPT in fluorescein and other xanthenone derivatives.[49−51] A change of the major emission band positions for **2g** at low and high buffer concentrations at a pH ∼ 4.6, λ_{em}^{max} = 631 nm (c_{buffer} = 0.03 M) and 692 nm (c_{buffer} = 3 M), corresponding to the emission from the forms B and A, respectively (Table 2), suggests that a high buffer concentration pronounces protonation of the basic form in the excited state, thus pK_b* < pK_b. Relatively low buffer concentrations used in our study did not apparently allow for an efficient ESPT within the lifetime of the fluorophores; nevertheless, the relative intensity of the emission could still affect some imaging applications, especially when working with buffers at pHs close the pK_a of the probes.

Our calculations qualitatively reproduce the trends for the experimental Stokes shifts (Table 3). They show that substantial geometry reorganization, involving particularly a change in the C9−N bond length (*j*), follows the photoexcitation of **1** and **2** (Figures S74−S81). As a result, the fluorescence of **1** and **2** is similar to that of pyronins with simple 9-amino substituents (for example, in **7b**), although still hypsochromically shifted as a consequence of the excess negative charge on the C9-nitrogen atom. In addition, we found that the Franck−Condon factors for the 0−0 transition in **1** and **2** are small and, as a result, the 0−0 transitions should have a relatively low intensity in the experimental spectra (see, for example, in Figures 1−3). The absorption and fluorescence maxima related to the transitions from/to higher vibrational levels are therefore more separated, elevating the Stokes shifts.

Dyes with very large Stokes shifts allow bioimaging applications of one excitation source and several different fluorescence channels without burden of spectral overlap artifacts (bleed-through or crosstalk).[52] However, such dyes often exhibit low fluorescence quantum yields, although it has been demonstrated that an intramolecular charge transfer (ICT)[53,54] or excited-state proton transfer[55] can also be responsible for bathochromic shifts in the absorption and emission spectra as well as large Stokes shifts.[18] The remarkably large Stokes shift values up to 208 nm (9130 cm^{-1}) in protic solvents, together with high brightness, $\varepsilon\Phi$, in the range of 6.2 and 8.6 × 10^3 dm^3 mol^{-1} cm^{-1} and absorption in the visible part of the spectrum at λ_{abs}^{max} ∼ 450 nm (Tables 1 and 2), introduce 9-imino-Si-pyronins as very promising candidates not only for

dx.doi.org/10.1021/jo502213t | J. Org. Chem. 2015, 80, 1299−1311

common fluorescent labeling experiments but particularly for multicolor confocal and STED microscopy applications. Special optical properties of these compounds are apparent from their comparison with those of the monochromophoric transition-metal-free small-organic molecule fluorophores with, to our knowledge, the largest Stokes shifts reported in the literature and several well-known and widely used xanthene and pyronin dyes (Figure 8). The emission properties of our pyronin derivatives in the acidic form A (**2f** in Figure 8) are comparable to those of the common very bright fluorophores ($\varepsilon\Phi$ over 10^4 dm^3 mol^{-1} cm^{-1}), such as sulforhodamine 101 (**i**)[56] (compare to Texas red[57]) or fluorescein (**ii**),[58,59] possessing only small Stokes shifts. The majority of fluorophores with large Stokes shifts absorb in the UV region, possess relatively low ε values, and are insoluble in water or fluoresce with small quantum yields, for example, a *N*-borylated pyrrol derivative **xi**.[60] Figure 8 also presents commercially available dyes ATTO 430LS (**v**), ATTO 490LS (**vii**),[61] and a pyronin analogue AZ 312 (**vi**).[34] As a result, our 9-imino-Si-pyronins (especially **2f**, Figure 8) are, to our knowledge, dyes with one of the largest Stokes shifts reported to date with fluorophore brightness above 10^3 dm^3 mol^{-1} cm^{-1}.

Due to favorable spectral properties of our 9-imino-Si-pyronins, we decided to closely investigate the Si-pyronin analogues which, moreover, represent a new class of fluorophores. The acid−base properties studied by optical spectroscopy provided reliable pK_a values to identify and assign the corresponding acid−base forms A and B. An additional NMR analysis in a buffered CD_3OD/D_2O mixture showed similar results. A low pK_a (~3) of 9-(sulfonylimino)-Si-pyronins implied that the compounds attain a neutral form B in aqueous solutions at practically all biologically relevant values of pH. Only 9-(acylimino)-Si-pyronins (**2c**,**f**) had a sufficiently high pK_a to allow us to observe a pure protonated form A. This form, with a formal single C9−N bond in its ground state, is characterized by the absorption and emission band maxima located in the red region and, in agreement with our calculations, a small Stokes shift (Table 3). The acid and base forms A and B were found to have a robust chemical stability and can repeatedly be switched from one to another by changing the solution pH (Figure 4 and Figure S36).

Finally, two water-soluble 2-deoxy-D-glucose derivatives, **2f**,**g**, prepared by a straightforward copper(I)-catalyzed azide−alkyne cycloaddition reaction (Scheme 2), were selected to demonstrate the simplicity of their implementation as "clickable" fluorescent probes.[3,65] The spectral properties of the fluorophores attached to a model saccharide were practically identical to those of the model compounds **2a**,**b**, thus the effect of a structural modification on the 9-imino group is negligible. The chemical stability of both **2f** and **2g** in DMSO in the dark was high ($\tau_{1/2} \gg$ 1 month) allowing their long-term storage in stock solutions. Their stability was lower in methanol and in a PBS buffer but still quite sufficient for a convenient manipulation with the solutions during the experiments (Table S1). Their good photostability (e.g., $\tau_{1/2}$ ~1 h for **2g** with LED or laser light sources; Table S2) in aqueous solutions fulfills an additional very important criterion[4] for utilizing these fluorophores under prolonged irradiation, for example, in fluorescence microscopy applications.

Thanks to their pK_a close to 7, the spectral properties of 9-(acylimino)-Si-pyronins can be easily altered by pH, and offer thus a potential for using these dyes as environmental pH indicators in aqueous media. Intracellular pH strongly affects the cell functions; therefore, it is of a great interest to measure pH qualitatively, particularly using a single-molecule probe.[66] On the other hand, 9-(sulfonylimino)-Si-pyronins are robust, stable and reliable fluorescent tags which are characterized by a high fluorophore brightness and outstanding and distinctive Stokes shifts under a wide span of solution pH.

CONCLUSION

We designed, synthesized, and both theoretically and experimentally studied several novel 9-(acylimino)- and 9-(sulfonylimino)-O- and Si-pyronin fluorophores. These compounds, especially the Si-analogues, exhibit remarkably high Stokes shifts (around 200 nm) while possessing a high fluorophore brightness, absorption bands in the near-UV and visible part of the spectrum, and high thermal and photochemical stabilities in protic solvents. We elucidated using quantum chemical calculations that the observed large Stokes shifts are related to the excitation of an electron from the HOMO to the LUMO of the chromophore that leads both to elongation of the C9−N bond and significant solvent reorganization. The photophysical properties of the compounds, their facile and high-yielding synthesis, and a simple protocol for their bioorthogonal ligation to a model saccharide using a Huisgen alkyne−azide cycloaddition predestine 9-iminopyronins for biochemical and biological applications as fluorescent tags and indicators for multichannel imaging, and for optoelectronic and dye laser applications. In addition, the spectral properties of 9-acyliminopyronins are shown to be alterable by solution pH, which is a significant value-added potential for their applications as pH sensors.

EXPERIMENTAL SECTION

Materials and Methods. The reagents and solvents of the highest purity available were used as purchased, or they were purified/dried when necessary. Acetonitrile, dichloromethane and tetrahydrofuran were dried by standard procedures, kept over activated 3 Å molecular sieve (8−12 mesh) under dry N_2; they were freshly distilled for each experiment. Phosphate buffer saline (PBS) was prepared by a 1:10 dilution of the stock solution (prepared by direct weighting of NaCl (80 g), KCl (2.0 g), $Na_2HPO_4{\cdot}12H_2O$ (23 g) and KH_2PO_4 (2.4 g) into a volumetric flask which was filled with distilled water to 1 L). The deuterated aqueous methanol-based phosphate buffers were prepared by titration of the aliquots prepared as a mixture of 120 μL of a stock solution (obtained by direct weighting of Na_3PO_4 (82.0 mg) into a volumetric flask which was filled with D_2O to 5 mL) and 480 μL of CD_3OD with DCl (either 0.1 mol dm^{-3} or 0.01 mol dm^{-3}; I = 0.1 mol dm^{-3}, KCl). Synthetic steps were performed under ambient atmosphere unless stated otherwise. All glassware was oven-dried prior to use when water- and/or air-sensitive reagents were used. In selected cases, the Schlenk techniques were used for work with air and/or moisture sensitive chemicals. All column chromatography purification procedures were performed on columns packed with silica.

NMR spectra were recorded on 300 or 500 MHz spectrometers in acetonitrile-d_3, chloroform-*d*, dimethyl sulfoxide-d_6, methanol-d_4, water-d_2, or their mixtures. The signals in ^{1}H and ^{13}C NMR spectra were referenced[67] to the residual peak of the (major) solvent except for D_2O, while those of the ^{19}F NMR were unreferenced and those of ^{29}Si NMR were referenced to TMS. The ^{15}N shifts were obtained from ^{1}H−^{15}N g-HMBC and were referenced to the nitrogen signal of acetonitrile-d_3 as a solvent (δ = 246 ppm).[68] The deuterated solvents (except for D_2O) were kept over activated 3 Å molecular sieve (8−12 mesh) under dry N_2. Mass spectra were recorded on a GC-coupled (30 m DB-XLB column) spectrometer in a positive mode with EI (70 eV). UV−vis spectra were obtained with matched 1.000 cm quartz cells. Fluorescence was measured on an automated luminescence spectrometer in 1.0 cm quartz fluorescence cuvettes at 25 ± 1 °C; the sample concentration was set to keep the absorbance below 0.1 at λ_{max}; each sample was measured five times, and the spectra were averaged. Emission and excitation spectra are normalized; they were corrected using standard correction files.

dx.doi.org/10.1021/jo502213t | J. Org. Chem. 2015, 80, 1299−1311

Scheme 5. Synthesis of 10 and 13

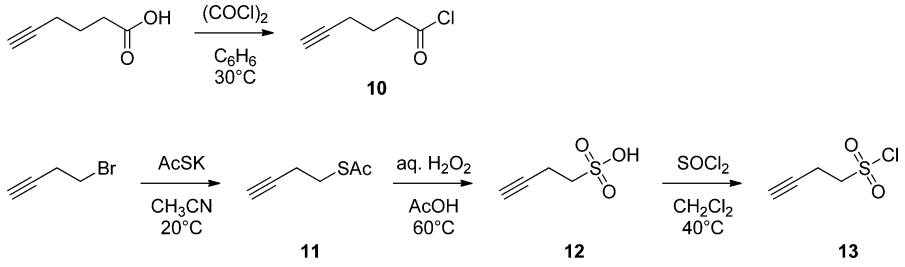

Fluorescence quantum yields were determined as the absolute values in 1.0 cm quartz fluorescence cuvettes at 25 ± 1 °C using an integration sphere. For each sample, the quantum yield was measured five times, and the values were averaged. Nanosecond flash lamp (filled with H_2) was used for measuring the fluorescence lifetimes. The data obtained were reconvoluted from measured decay curves of the sample and the instrumental response function. IR spectra were obtained on an FT-IR spectrometer from the KBr pellets or using an ATR mode. Exact masses were obtained using a spectrometer equipped with a time-of-flight mass analyzer in positive ion mode. Melting points were obtained using a noncalibrated Kofler's hot stage melting point apparatus. The solution pH values were determined using a glass electrode calibrated with certified buffer solutions at pH = 4, 7, or 10. A global analysis software was used for determination of the pK_a values from a series of absorption spectra measured in aqueous solutions (I was kept constant at 0.1 mol dm^{-3} using KCl when necessary) of the compounds.

Quantum-Chemical Calculations. All calculations were carried out with the Gaussian 09 suite of electronic structure programs.[69] The ground- and excited-state geometries were optimized with the (TD)-PBE0[70] density functional and the 6-31+G(d) basis set, which was shown to perform satisfactorily in a number of studies that modeled the absorption and emission spectra as well as the Stokes shifts.[71,72] A tighter DFT integration grid was used in all calculations. The collective effects of the surrounding solvent were modeled within the polarizable continuum model (PCM) with methanol as a solvent. State-specific nonequilibrium solvation was used in calculations of vertical excitation energies, while equilibrium solvation was used in geometry optimizations. Analytical and numerical frequency analysis was performed to verify that all structures correspond to true minima on the ground and the excited potential energy surfaces (PES), respectively, and to provide the zero-point vibrational energy (ZPVE) corrections that has not been scaled. Single point energies of the dyes on the ground state PES were computed at the PBE0/6-311+G(2df,p) level of theory in PCM to assess the energies of different conformations. The final energies in the conformational analysis are the sum of the single point energies and the ZPVEs. ZPVEs were also added to the TD-PBE0 vertical excitation energies to provide the energies of absorption and fluorescence. Calculations of vibrationally resolved spectra were performed using the FCclasses program[27] with the default settings of the program in Gaussian 09.

Synthetic Procedures. *Hex-5-ynoyl Chloride (**10**; Scheme 5).* This procedure is a modification of that reported by Vollhardt.[73] Oxalyl chloride (8.5 g, 67 mmol) was added dropwise to a stirred solution of hex-5-ynoic acid (5.0 g, 44.6 mmol) in benzene (50 mL) at 20 °C. The resulting solution was stirred at 30 °C for 2 h. The solvent was removed under reduced pressure, and the residue was distilled on a Kugelrohr apparatus to give the title product. Yield: 3.71 g (64%). Colorless liquid with pungent odor. Bp: 65 °C (1 mmHg) (lit.[73] bp 50−55 °C). ^{1}H NMR (300 MHz, $CDCl_3$): δ (ppm) 1.88−1.96 (m, 2H), 2.02 (t, 1H, J = 2.6 Hz, C≡C−**H**), 2.31 (dt, 2H, J_1 = 6.7 Hz, J_2 = 2.7 Hz), 3.07 (t, 2H, J = 7.2 Hz). ^{13}C NMR (75.5 MHz, $CDCl_3$): δ (ppm) 17.4, 23.9, 45.8, 70.2, 82.4, 173.6. This compound has also been characterized elsewhere.[73,74]

*S-But-3-yn-1-yl Ethanethiolate (**11**; Scheme 5).* A solution of 4-bromobut-1-yne (1.0 g, 7.5 mmol) and potassium ethanethiolate (2.6 g, 22.6 mmol) in acetonitrile (50 mL) was stirred at 20 °C for 20 h. The reaction mixture was filtered; the volatiles were removed under reduced pressure to give a brown oil which was used in the next step without further purification. Yield: 0.80 g (83%). Brown oil. ^{1}H NMR (300 MHz, $CDCl_3$): δ (ppm) 3.03 (t, 2H, J = 7.1 Hz), 2.47 (td, 2H, J_1 = 7.1 Hz, J_2 = 2.6 Hz,), 2.34 (s, 3H), 2.01 (t, 1H, J = 2.6 Hz, C≡C−H). ^{13}C NMR (75.5 MHz, $CDCl_3$): δ (ppm) 19.6, 28.2, 30.7, 69.7, 82.2, 195.3. FTIR (ATR, cm^{-1}): 3291, 2941, 2120 (weak, C≡C), 1686 (C═O), 1428, 1354, 1130, 974, 945, 619, 535, 466. MS (EI): 127 (33), 113 (100), 86 (47), 85 (36), 53 (24). This compound has also been characterized elsewhere.[75]

*But-3-yne-1-sulfonic Acid (**12**; Scheme 5).* Aqueous solution of hydrogen peroxide (30%, v/v, 3.84 mL, 37.6 mmol) was added dropwise to a solution of *S*-but-3-yn-1-yl ethanethiolate (**11**, 0.80 g, 6.22 mmol) in acetic acid (10 mL), and the reaction mixture was stirred at 60 °C for 1 h until no starting material was observed by GC. The reaction mixture was then cooled down to 20 °C, and the volatiles were removed under reduced pressure. The traces of acetic acid were removed by azeotropic distillation with *n*-heptane (2 × 10 mL). The resulting title product was used in the next step without further purification. Yield: 0.70 g (84%). Colorless oil. ^{1}H NMR (300 MHz, D_2O): δ (ppm) 2.39 (t, 1H, J = 2.6 Hz, C≡C−H), 2.63 (td, 2H, J_1 = 7.4 Hz, J_2 = 2.6 Hz), 3.08 (t, 2H, J = 7.4 Hz). This compound has also been reported elsewhere.[76]

*But-3-yne-1-sulfonyl Chloride (**13**; Scheme 5).* A solution of thionyl chloride (2.7 mL, 37 mmol), but-3-yne-1-sulfonic acid (**12**, 0.73 g, 5.4 mmol) and dimethylformamide (0.1 mL) in dry dichloromethane (1.8 mL) was refluxed under N_2 atmosphere for 5 h. The reaction mixture was then cooled down to 20 °C, and the volatiles were removed under reduced pressure. The resulting residue was distilled on a Kugelrohr apparatus to give the pure title product which was used in the next step. Yield: 0.11 g (13%). Colorless oil. Bp: 55−60 °C (1 mmHg) (lit.[76] 44−45 °C, 0.5 mmHg). ^{1}H NMR (300 MHz, $CDCl_3$): δ (ppm) 2.17 (t, 1H, J = 2.7 Hz, C≡C−H), 2.96 (td, 1H, J_1 = 7.7, J_2 = 2.7 Hz), 3.86 (t, 1H, J = 7.7 Hz). FTIR (ATR, cm^{-1}) = 3296, 2995, 2934, 1737, 1368, 1164, 657, 592, 530, 474, 447. This compound has also been reported elsewhere.[76]

Scheme 6. Synthesis of 5

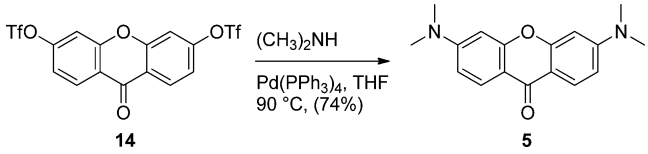

*9-Oxo-9H-xanthene-3,6-diyl Bis(trifluoromethanesulfonate) (**14**; Scheme 6).* Compound **14** was prepared according to previously published procedure.[77]

*3,6-Bis(dimethylamino)-9H-xanthen-9-one (**5**).* Tetrakis-(triphenylphosphino)palladium (100 mg, 0.142 mmol) was added in one portion to a solution of 9-oxo-9*H*-xanthene-3,6-diyl bis-(trifluoromethanesulfonate) (**14**, 1.00 g, 2.03 mmol) in dry tetrahydrofuran (20 mL) in a high-pressure glass tube, and the reaction mixture was cooled to −78 °C. Liquid dimethylamine (4.0 mL, 60 mmol) was subsequently added to the reaction mixture in one portion, and the vessel was sealed. The reaction mixture was stirred overnight at 90 °C and then cooled to 20 °C. Water (20 mL) was added, and tetrahydrofuran was removed under reduced pressure. Yellow

dx.doi.org/10.1021/jo502213t | J. Org. Chem. 2015, 80, 1299−1311

suspension of the crude product was filtered and subsequently washed with cold water (5 mL) and cold *n*-hexane (3 × 2 mL). The filtrate was dried under high vacuum and used in next step without any purification. Yield: 423 mg (74%). Slightly yellow powder. Mp: 262−264 °C (lit.[37] 235−242 °C). ^{1}H NMR (500 MHz, $CDCl_3$): δ (ppm) 3.10 (s, 12H), 6.48 (d, 2H, J = 2.4 Hz), 6.90 (dd, 2H, J_1 = 9.0 Hz, J_2 = 2.4 Hz), 8.14 (d, 2H, J = 9.0 Hz) (Figure S2). ^{13}C NMR (125 MHz, $CDCl_3$): δ (ppm) 40.4, 97.3, 109.2, 112.3, 127.9, 154.6, 158.4, 176.4 (Figure S3). FTIR (KBr, cm^{-1}) = 2905, 2807, 1602, 1532, 1432, 1351, 1331, 1255, 1159, 1121, 808, 709, 668. MS (EI): 282 (100), 265 (15), 236 (6), 222 (4), 194 (3), 166 (4), 140 (17), 127 (19), 111 (9), 97 (14), 83 (15), 70 (16), 57 (18). UV−vis (CH_3OH, $c = 1.0 \times 10^{-4}$ mol dm^{-3}): λ_{max} (log ε) = 379 (4.24) nm (dm^3 mol^{-1} cm^{-1}) (Figure S4). Fluorescence (CH_3OH, A (λ_{max} (excitation)) ≤ 0.1): λ_{max} (emission) = 442 nm (Figure S4). HRMS (APCI$^+$−TOF) m/z: $[M + H]^+$ calcd for $C_{17}H_{19}N_2O_2$ 238.1441; found: 283.1442. This compound has also been characterized elsewhere.[37]

Note: The noncatalyzed Buchwald−Hartwig amination of 9-oxo-9*H*-xanthene-3,6-diyl bis(trifluoromethanesulfonate) (**14**) with piperidine leads to 3,6-di(piperidin-1-yl)-9*H*-xanthen-9-one in high yield (>90%).[20,77] However, we found that dimethylamine does not react under these conditions, and **5** is formed only upon addition of a Pd-catalyst (in 74% yield using 7 mol % of $Pd(PPh_3)_4$ and in 54% yield using 7 mol % of $PdCl_2(PPh_3)_2$).

*3,7-Bis(dimethylamino)-5,5-dimethyldibenzo[b,e]silin-10(5H)-one (**6**).* This compound was prepared according to a previously published procedure.[22] ^{29}Si NMR (99.3 MHz, $CDCl_3$): δ (ppm) −23.3 (s) (Figure S5). IR, see ref.[22] (Figure S6). UV−vis (CH_3OH, c = 4.4 × 10^{-5} mol dm^{-3}): λ_{max} (log ε) = 402 (4.51) nm (dm^3 mol^{-1} cm^{-1}) (Figure S10). Fluorescence (CH_3OH, A (λ_{max} (excitation)) ≤ 0.1): λ_{max} (emission) = 489 nm (Figure S10).

*Synthesis of 9-Aminopyronin Analogues **3** and **4**: A General Procedure.* Trifluoromethanesulfonic anhydride (2.2 g, 1.3 mL, 7.7 mmol) was added dropwise to a stirred solution of ketone (**5** or **6**, 1.54 mmol) in dry dichloromethane (15 mL) in a Schlenk flask under dry N_2 atmosphere. The reaction mixture was stirred at 20 °C for 15 min, and gaseous ammonia was then bubbled through this solution for 10 min which was accompanied by a change of color. The reaction mixture was further stirred under the ammonia atmosphere for 10 h. The mixture was subsequently bubbled through with nitrogen to remove excess of ammonia, and water (20 mL) was added in one portion. The reaction mixture was acidified by careful addition of trifluoromethanesulfonic acid to adjust the pH to ∼1, washed with water (2 × 20 mL), aq $NaHCO_3$ (5%, w/w, 2 × 20 mL) and brine (20 mL), dried over anhydrous magnesium sulfate and filtered. The volatiles were removed under reduced pressure, and the resulting colored crystalline solid was chromatographed (CH_3OH/CH_2Cl_2, 1:19, v/v) to give the pure product.

*N-(9-Amino-6-(dimethylamino)-3H-xanthen-3-ylidene)-N-methylmethanaminium Trifluoromethanesulfonate (**3**).* This compound was synthesized from **5** and ammonia. Yield: 473 mg (85%). Yellow crystalline solid. Mp: >250 °C. ^{1}H NMR (500 MHz, CD_3CN): δ (ppm) 3.13 (s, 12H), 6.50 (d, 2H, J = 2.5 Hz), 6.90 (dd, 2H, J_1 = 9.4 Hz, J_2 = 2.5 Hz), 7.68 (bs, 2H, −NH_2), 7.78 (d, 2H, J = 9.4 Hz) (Figure S11). ^{13}C NMR (126 MHz, CD_3CN) δ (ppm) 40.6, 97.2, 101.8, 112.6, 121.0 (q, $^1J_{C-F}$ = 321 Hz), 126.4, 156.0, 157.1, 157.7 (Figure S12). ^{15}N NMR (CD_3CN) δ 75 (−N(CH_3)$_2$), 98 (−$N$$H_2$) (ppm) (Figure S13). ^{19}F NMR (282 MHz, $CDCl_3$): δ (ppm) −80.2 (s). MS (EI): m/z = 281 (75), 264 (15), 239 (15), 226 (15), 127 (30), 97 (40), 85 (65), 57 (95), 43 (100). FTIR (cm^{-1}): 3419, 3363, 3270, 2920, 1638, 1588, 1532, 1482, 1440, 1342, 1181, 1134, 1052, 814, 610, 567, 506. UV−vis (CH_3OH, $c = 5 \times 10^{-5}$ mol dm^{-3}): λ_{max} = 237, 290, 342, 432 nm (Figure S14). Fluorescence (CH_3OH, A (λ_{max} (excitation)) ≤ 0.1): λ_{max} (emission) = 478 nm (Figure S14). UV−vis (basic CH_3OH, c = 5 × 10^{-5} mol dm^{-3}): λ_{max} = 234, 273, 292, 353 nm (Figure S15). Fluorescence (basic CH_3OH, A (λ_{max} (excitation)) ≤ 0.1): λ_{max} (emission) = 482 nm (Figure S15). HRMS (APCI$^+$−TOF) m/z: $[M]^+$ calcd for $C_{17}H_{20}N_3O$ 282.1601; found 282.1597.

*N-(10-Amino-7-(dimethylamino)-5,5-dimethyldibenzo[b,e]silin-3(5H)-ylidene)-N-methylmethanaminium Trifluoromethanesulfonate (**4**).* This compound was synthesized from **6** and ammonia. Yield: 715 mg (98%). Red crystalline solid. Mp: 42.7−43.1 °C. ^{1}H NMR (500 MHz, CD_3CN): δ (ppm) 0.46 (s, 6H, >Si(CH_3)$_2$), 3.14 (s, 12H), 6.89 (dd, 2H, J_1 = 9.2 Hz, J_2 = 2.6 Hz), 7.02 (d, 2H, J = 2.7 Hz), 7.90 (d, 2H, J = 9.2 Hz), 8.54 (bs, 2H, −NH_2) (Figure S16). ^{13}C NMR (126 MHz, CD_3CN) δ (ppm) −1.6 (>Si(CH_3)$_2$), 40.4, 114.3, 117.5, 120.1, 121.0 (q, $^1J_{C-F}$ = 321 Hz), 131.3, 144.3, 154.1, 169.5 (Figure S17). ^{15}N NMR (CD_3CN) δ 71 (−N(CH_3)$_2$), 127 (−NH_2) (ppm) (Figures S18 and S19). ^{19}F NMR (282 MHz, $CDCl_3$): δ (ppm) −78.6 (s). MS (EI): m/z = 323 (100), 308 (85), 236 (23), 148 (32), 123 (21), 111 (36), 97 (67), 83 (84). FTIR (cm^{-1}): 3332, 3180, 2920, 1692, 1579, 1356, 1256, 1146, 1111, 1057, 1033, 827, 759, 633, 553, 516 (Figure S20). HRMS (APCI$^+$−TOF) m/z: $[M]^+$ calcd for $C_{19}H_{26}N_3Si$ 324.1891; found 324.1896.

*Synthesis of 9H-Xanthene Amide-3,6-diamine Derivatives (**1**) and their Si-Analogues **2**: General Procedure.* A solution of acyl chloride or sulfonyl chloride (0.170 mmol) in dry dichloromethane (2 mL) was added dropwise to a stirred solution of a 9-aminopyronin (**3** or **4**, 0.140 mmol) and triethylamine (0.072 g, 0.1 mL, 0.710 mmol) in dry dichloromethane (3 mL) at 20 °C, and the reaction mixture was stirred under dry N_2 atmosphere for 2 h. The mixture was then diluted with dichloromethane (10 mL), washed with water (2 × 10 mL), brine (10 mL), dried over anhydrous magnesium sulfate, and filtered. Volatiles were removed under reduced pressure, and the resulting residue was chromatographed (*n*-hexane/ethyl acetate, 5:1, v/v) to give the pure product.

*N-(3,6-Bis(dimethylamino)-9H-xanthen-9-ylidene)acetamide (**1a**).* This compound was synthesized from acetyl chloride and **3**. Yield: 34 mg (74%). Red crystalline solid. Mp: 172−174 °C. ^{1}H NMR (500 MHz, $CDCl_3$): δ (ppm) 2.35 (s, 3H), 3.09 (s, 12H), 6.45 (d, 2H, J = 2.5 Hz), 6.63 (dd, 2H, J_1 = 9.1 Hz, J_2 = 2.5 Hz), 7.82 (d, 2H, J = 9.1 Hz) (Figure S22). ^{13}C NMR (126 MHz, $CDCl_3$): δ (ppm) 25.6, 40.1, 97.3, 107.9, 109.5, 128.5, 147.3, 154.0, 156.3, 182.6 (Figure S23). MS (EI): m/z = 323 (19), 308 (86), 292 (19), 280 (6), 264 (10), 236 (5), 154 (17), 43 (100). FTIR (cm^{-1}): 1597, 1578, 1527, 1426, 1257, 1231, 1181, 1132, 1053, 919, 806, 697, 655, 603, 569, 507. UV−vis (CH_3OH, c = 7.0 × 10^{-5} mol dm^{-3}): λ_{max} (log ε) = 202 (4.20), 237 (4.53), 278 (4.03), 376 (4.32) nm (dm^3 mol^{-1} cm^{-1}) (Figure S24). Fluorescence (CH_3OH, A (λ_{max} (excitation)) ≤ 0.1): λ_{max} (emission) = 513 nm (Figure S24). UV−vis (1% HCl in CH_3OH (v/v), $c = 6.4 \times 10^{-6}$ mol dm^{-3}): λ_{max} = 237, 253, 296, 359, 549 nm (Figure S25). Fluorescence (1% HCl in CH_3OH (v/v), A (λ_{max} (excitation)) ≤ 0.1): λ_{max} (emission) = 576 nm (Figure S25). HRMS (ESI$^+$): calcd for $C_{19}H_{22}N_3O_2^+$ $[M + H]^+$ 324.1707; found 324.1704.

*N-(3,6-Bis(dimethylamino)-9H-xanthen-9-ylidene)methanesulfonamide (**1b**).* This compound was synthesized from methanesulfonyl chloride and **3**. Yield: 28 mg (84%). Orange crystalline solid. Mp: >250 °C. ^{1}H NMR (300 MHz, $CDCl_3$): δ (ppm) 3.13 (s, 12H), 3.31 (s, 3H), 6.46 (d, 2H, J = 2.6 Hz), 6.74 (dd, 2H, J_1 = 9.4 Hz, J_2 = 2.6 Hz), 8.55 (d, 2H, J = 9.4 Hz) (Figure S26). ^{13}C NMR (75.5 MHz, $CDCl_3$): δ (ppm) 40.3, 45.1, 96.7, 109.2, 109.9, 131.0, 154.7, 157.3, 157.7 (Figure S27). MS (EI): m/z = 359 (100), 344 (27), 294 (14), 281 (38), 252 (36), 236 (31), 140 (17), 127 (49), 42 (4). FTIR (cm^{-1}): 2918, 2852, 1644, 1594, 1528, 1494, 1354, 1323, 1263, 1125, 1105, 966, 897, 844, 823, 802, 766, 658, 593, 510. UV−vis (CH_3OH, $c = 5.0 \times 10^{-5}$ mol dm^{-3}): λ_{max} (log ε) = 422 (4.19) nm (dm^3 mol^{-1} cm^{-1}) (Figure S28). Fluorescence (CH_3OH, A (λ_{max} (excitation)) ≤ 0.1): λ_{max} (emission) = 525 nm (Figure S28). HRMS (APCI$^+$−TOF) m/z: $[M + H]^+$ calcd for $C_{18}H_{22}N_3O_3S$ 360.1376; found 360.1373.

*N-(3,7-Bis(dimethylamino)-5,5-dimethyldibenzo[b,e]silin-10(5H)-9-ylidene)acetamide (**2a**).* This compound was synthesized from acetyl chloride and **4**. Yield: 48 mg (92%). Green crystalline solid. Mp: 131−133 °C. ^{1}H NMR (500 MHz, $CDCl_3$): δ (ppm) 0.48 (s, 6H, >Si(CH_3)$_2$), 2.07 (s, 3H), 3.06 (s, 12H), 6.75 (dd, 2H, J_1 = 8.9 Hz, J_2 = 2.8 Hz), 6.85 (d, 2H, J = 2.8 Hz), 7.91 (d, 2H, J = 8.9 Hz) (Figure S29). ^{13}C NMR (126 MHz, $CDCl_3$): δ (ppm) −1.4 (>Si(CH_3)$_2$), 25.7, 40.2, 113.3, 115.0, 129.6, 130.6, 138.4, 150.7, 159.4, 184.0, (Figure S30). ^{15}N NMR (CD_3CN) δ (ppm) 54 (−N(CH_3)$_2$), 321 (=NCOCH_3) (Figure S32). MS (EI): m/z = 365 (19), 351 (29), 350 (100), 334 (13). FTIR (cm^{-1}): 2951, 2922, 2805, 1658, 1575, 1493, 1445, 1354, 1296, 1223,

dx.doi.org/10.1021/jo502213t | J. Org. Chem. 2015, 80, 1299−1311

1175, 1150, 1060, 836, 780, 757, 701, 661, 644, 611, 556, 470, 441 (Figure S33). UV−vis (CH_3OH, $c = 7.4 \times 10^{-5}$ mol dm^{-3}): λ_{max} (log ε) = 215 (4.48), 254 (4.22), 387 (4.24) nm (dm^3 mol^{-1} cm^{-1}) (Figure S36). Fluorescence (CH_3OH, A (λ_{max} (excitation)) ≤ 0.1): λ_{max} (emission) = 597 nm (Figure S36). UV−vis (1% HCl in CH_3OH (v/v), $c = 2.4 \times 10^{-5}$ mol dm^{-3}): λ_{max} = 322, 428, 658 nm (Figure S37). Fluorescence (1% HCl in CH_3OH (v/v), A (λ_{max} (excitation)) ≤ 0.1): λ_{max} (emission) = 679 nm (Figure S37). HRMS (APCI$^+$−TOF) m/z: $[M + H]^+$ calcd for $C_{21}H_{28}N_3OSi$ 366.1996; found 366.1994.

*N-(3,7-Bis(dimethylamino)-5,5-dimethyldibenzo[b,e]silin-10(5H)-ylidene)methanesulfonamide (**2b**).* This compound was synthesized from methanesulfonyl chloride and **4**. Yield: 35 mg (82%). Orange crystalline solid. Mp: 219−221 °C. ^{1}H NMR (500 MHz, $CDCl_3$): δ (ppm) 0.49 (s, 6H, >Si(CH_3)$_2$), 3.08 (s, 12H), 3.19 (s, 3H), 6.77 (dd, 2H, J_1 = 9.0 Hz, J_2 = 2.8 Hz), 6.83 (d, 2H, J = 2.8 Hz), 8.26 (d, 2H, J = 9.0 Hz) (Figure S41). ^{13}C NMR (126 MHz, $CDCl_3$): δ (ppm) −1.6 (>Si(CH_3)$_2$), 40.1, 44.6, 112.3, 114.8, 129.0, 132.8, 139.4, 151.3, 174.0 (Figure S42). ^{15}N NMR (CD_3CN) δ (ppm) 58 (−N(CH$_3$)$_2$), 281 (=NSO$_2$CH$_3$) (Figure S43). MS (EI): m/z = 401 (91), 386 (60), 372 (7), 336 (59), 322 (100), 307 (53), 292 (29), 278 (28), 263 (19), 249 (7), 161 (33), 147 (31). FTIR (cm^{-1}): 2934, 1584, 1548, 1476, 1365, 1182, 1120, 1063, 968, 836, 760, 575, 526 (Figure S44). UV−vis (CH_3OH, $c = 6.2 \times 10^{-5}$ mol dm^{-3}): λ_{max} (log ε) = 213 (4.34), 248 (4.03), 388 (4.05), 444 (4.17) nm (dm^3 mol^{-1} cm^{-1}) (Figure S47). Fluorescence (CH_3OH, A (λ_{max} (excitation)) ≤ 0.1): λ_{max} (emission) = 617 nm (Figure S47). HRMS (APCI$^+$−TOF) m/z: $[M + H]^+$ calcd for $C_{20}H_{28}N_3O_3SSi$ 402.1666; found 402.1668. pK_a (nonbuffered aqueous solution, I = 0.1 mol dm^{-3}) ∼ 2.8 ± 0.2.

*N-(3,7-Bis(dimethylamino)-5,5-dimethyldibenzo[b,e]silin-10(5H)-ylidene-2-(2-(2-methoxyethoxy)ethoxy)acetamide (**2c**).* This compound was synthesized from 2-(2-(2-methoxyethoxy)ethoxy)acetyl chloride and **4**. Yield: 68 mg (83%). Green highly viscous oil. ^{1}H NMR (500 MHz, $CDCl_3$): δ (ppm) 0.47 (s, 6H, >Si(CH_3)$_2$), 3.04 (s, 12H), 3.32 (s, 3H), 3.46−3.44 (m, 2H), 3.54−3.50 (m, 4H), 3.62−3.59 (m, 2H), 4.08 (s, 2H), 6.72 (dd, 2H, J_1 = 8.9 Hz, J_2 = 2.8 Hz), 6.82 (d, 2H, J = 2.8 Hz), 7.91 (d, 2H, J = 8.9 Hz) (Figure S49). ^{13}C NMR (126 MHz, $CDCl_3$): δ (ppm) −1.4 (>Si(CH_3)$_2$), 40.0, 59.0, 70.4, 70.5, 70.8, 71.4, 71.9, 113.1, 114.9, 129.2, 130.9, 138.7, 150.8, 161.7, 181.8 (Figure S50). MS (EI): m/z = 484 (11), 470 (10), 350 (100), 334 (82), 323 (28), 320 (21), 309 (21), 292 (16), 263 (10), 175 (35), 102 (4), 59 (22). FTIR (cm^{-1}): 2875, 2812, 1643 (C=O), 1578, 1495, 1445, 1357, 1296, 1246, 1176, 1104, 1059, 960, 926, 838, 782, 759, 700, 677, 577, 505, 445. UV−vis (CH_3OH, $c = 3.3 \times 10^{-5}$ mol dm^{-3}): λ_{max} (log ε) = 400 (4.42) nm (dm^3 mol^{-1} cm^{-1}) (Figure S51). Fluorescence (CH_3OH, A (λ_{max} (excitation)) ≤ 0.1): λ_{max} (emission) = 596 nm (Figure S51). HRMS (ESI$^+$−TOF) m/z: $[M + H]^+$ calcd for $C_{26}H_{38}N_3O_4Si$ 484.2626; found 484.2623. pK_a (nonbuffered aqueous solution, I = 0.1 mol dm^{-3}) = 6.77 ± 0.06.

*N-(3,7-Bis(dimethylamino)-5,5-dimethyldibenzo[b,e]silin-10(5H)-ylidene)hex-5-ynamide (**2d**).* This compound was synthesized from hex-5-ynoyl chloride (**10**) and **4**. Yield: 53 mg (89%). Green wax. ^{1}H NMR (500 MHz, $CDCl_3$): δ (ppm) 0.49 (s, 6H, >Si(CH_3)$_2$), 1.83 (p, 2H, J = 7.2 Hz), 1.84 (t, 1H, J = 2.6 Hz), 2.20 (td, 2H, J_1 = 7.1 Hz, J_2 = 2.6 Hz), 2.42 (t, 2H, J = 7.4 Hz), 3.06 (s, 12H), 6.74 (dd, 2H, J_1 = 9.0 Hz, J_2 = 2.8 Hz), 6.84 (d, 2H, J = 2.8 Hz), 7.90 (d, 2H, J = 9.0 Hz) (Figure S53). ^{13}C NMR (126 MHz, $CDCl_3$): δ (ppm) −1.4 (>Si(CH_3)$_2$), 18.2, 24.3, 37.2, 40.2, 68.7, 84.0, 113.2, 115.0, 129.7, 130.7, 138.5, 150.7, 159.3, 185.4 (Figure S54). MS (EI): m/z = 417 (9), 350 (73), 324 (100), 309 (76), 293 (24), 193 (16), 175 (15), 148 (36), 43 (21). FTIR (cm^{-1}): 3291, 2901, 2809, 2116 (weak, C≡C), 1620, 1581, 1496, 1446, 1358, 1297, 1247, 1229, 1176, 1126, 1062, 961, 926, 768, 642, 576, 442. UV−vis (CH_3OH, $c = 4.0 \times 10^{-5}$ mol dm^{-3}): λ_{max} (log ε) = 387 (4.40) nm (dm^3 mol^{-1} cm^{-1}) (Figure S55). Fluorescence (CH_3OH, A (λ_{max} (excitation)) ≤ 0.1): λ_{max} (emission) = 595 nm (Figure S55). UV−vis (PBS/DMSO, 99:1, v/v, c = ∼ 1×10^{-5} mol dm^{-3}): λ_{max} = 408 nm (dm^3 mol^{-1} cm^{-1}). Fluorescence (PBS/DMSO, 99:1, v/v, A (λ_{max} (excitation)) ≤ 0.1): λ_{max} (emission) = 605 nm. HRMS (APCI$^+$−TOF) m/z: $[M + H]^+$ calcd for $C_{25}H_{31}N_3OSi$ 418.2309; found 418.2304.

*N-(3,7-Bis(dimethylamino)-5,5-dimethyldibenzo[b,e]silin-10(5H)-ylidene)but-3-yne-1-sulfonamide (**2e**).* This compound was synthesized from but-3-yne-1-sulfonyl chloride (**13**) and **4**. Yield: 23 mg (38%). Green crystalline solid. Mp: 86.7−88.1 °C. ^{1}H NMR (500 MHz, $CDCl_3$): δ (ppm) 0.48 (s, 6H, >Si(CH_3)$_2$), 1.97 (t, 1H, J = 2.7 Hz), 2.84 (ddd, 2H, J_1 = 8.3 Hz, J_2 = 6.1 Hz, J_3 = 2.7 Hz), 3.09 (s, 12H), 3.43 (m, 2H), 6.77 (dd, 2H, J_1 = 9.0 Hz, J_2 = 2.8 Hz), 6.82 (d, 2H, J = 2.8 Hz), 8.24 (d, 2H, J = 9.0 Hz) (Figure S56). ^{13}C NMR (126 MHz, $CDCl_3$): δ (ppm) −1.6 (>Si(CH_3)$_2$), 14.8, 40.1, 54.6, 69.8, 81.2, 112.3, 114.8, 129.8, 133.0, 139.6, 151.4, 174.8 (Figure S57). MS (EI): m/z = 442 (61), 392 (100), 377 (63), 293 (14), 281 (46), 182 (43), 154 (11). FTIR (cm^{-1}): 3286, 2921, 2249 (weak, C≡C), 1581, 1550, 1486, 1363, 1294, 1179, 1115, 1063, 869, 838, 762, 731. UV−vis (CH_3OH, $c = 4.8 \times 10^{-5}$ mol dm^{-3}): λ_{max} (log ε) = 213 (4.48), 247 (4.17), 392 (4.21), 452 (4.30) nm (dm^3 mol^{-1} cm^{-1}) (Figure S58). Fluorescence (CH_3OH, A (λ_{max} (excitation)) ≤ 0.1): λ_{max} (emission) = 617 nm (Figure S58). HRMS (APCI$^+$−TOF) m/z: $[M + H]^+$ calcd for $C_{29}H_{30}N_3O_2SSi$ 440.1823; found 440.1819.

*Azide−Alkyne Huisgen Cycloaddition of **2d** and **2e** with Azide: A General Procedure.* The procedure of Kim and co-workers was utilized.[21]

*N-(3,7-Bis(dimethylamino)-5,5-dimethyldibenzo[b,e]silin-10(5H)-ylidene)-4-(1-((4R,5S,6R)-2,4,5-trihydroxy-6-(hydroxymethyl)-tetrahydro-2H-pyran-3-yl)-1H-1,2,3-triazol-4-yl)butanamide (**2f**).* This compound was synthesized from **2d** and 2-azido-2-deoxy-D-glucose. Yield: 73 mg (91%). Orange crystalline solid. Mp: 127.7−128.5 °C. ^{1}H NMR (500 MHz, CD_3OD): δ (ppm) 0.45 (s, 6H, >Si(CH_3)$_2$), 1.94 (p, 2H, J = 7.3 Hz), 2.45 (t, 2H, J = 7.0 Hz), 2.70 (t, 2H, J = 7.7 Hz), 3.05 (s, 12H, −N(CH_3)$_2$), 3.41−3.55 (m, 1.5H), 3.72−3.82 (m, 1.2H), 3.85 (dd, 0.6H, J_1 = 11.4 Hz, J_2 = 2.1 Hz), 3.89−3.98 (m, 1.1H), 4.00−4.11 (m, 1.0H), 4.19−4.25 (m, 0.6H), 4.56 (dd, 0.6H, J_1 = 11.0 Hz, J_2 = 3.2 Hz), 4.80 (bs, 4H, −OH) 5.05 (d, 0.45H, J = 7.7 Hz, regioisomer a), 5.25 (d, 0.55H, J = 2.8 Hz, regioisomer b), 6.80 (dd, 2H, J_1 = 8.7 Hz, J_2 = 2.4 Hz), 6.93 (d, 2H, J = 2.4 Hz), 7.54 (s, 0.45H, =N−C(CH$_2$)=CH−N(glu)−, regioisomer a), 7.74 (s, 0.55H, =N−C(CH$_2$)=CH−N(glu)−, regioisomer b), 7.78 (d, 2H, J = 8.7 Hz) (Figure S59). ^{13}C NMR (126 MHz, $CDCl_3$): δ −1.5 (>Si(CH_3)$_2$), 25.9 (−CH_2−), 26.4 (−CH_2−), 38.6 (=NCOCH_2−), 40.2 (−N(CH_3)$_2$), 62.6 (glu: −CH_2OH, anomer 1), 62.7 (glu: CH_2OH, anomer 2), 66.8 (glu: >CHOH, anomer 1), 69.6 (glu: >CHOH, anomer 2), 71.7 (glu: >CHOH, anomer 1), 72.2 (glu: >CHOH, anomer 2), 72.5 (glu: >CHOH, anomer 1), 73.3 (glu: >CHOH, anomer 1), 75.5 (glu: >CHOH, anomer 2), 78.2 (glu: >CHOH, anomer 2), 92.8 (glu: −CH(OH)−O−, anomer 1), 96.2 (glu: −CH(OH)−O−, anomer 2), 114.2 (C_{ar}H), 116.3 (C_{ar}H), 122.6 (>C=CH−N(glu)−, regioisomer b), 124.5 (>C=CH−N(glu)−, regioisomer a), 131.7 ($C_{ar(q)}$), 140.3 (C_{ar}H), 142.6 (>C=CH−N(glu)−, regioisomer a), 142.8 (>C=CH−N(glu)−, regioisomer b), 152.5 ($C_{ar(q)}$), 161.1 (>C=N−C(=O)−), 186.6 (>C=O) (ppm) (Figure S60). MS (EI): m/z = 623 (M$^+$, not observed), 406 (<1), 337 (6), 323 (100), 308 (69), 294 (16), 281 (5), 193 (4), 160 (5), 148 (30), 108 (7), 96 (13), 53 (6). FTIR (cm^{-1}): 3342, 2924, 2897, 1623, 1583, 1497, 1446, 1361, 1303, 1247, 1229, 1178, 1121, 1062, 840, 781, 758, 700, 668, 562. UV−vis (CH_3OH, $c = 4.2 \times 10^{-5}$ mol dm^{-3}): λ_{max} (log ε) = 254 (4.32), 386 (4.34) nm (dm^3 mol^{-1} cm^{-1}) (Figure S61). Fluorescence (CH_3OH, A (λ_{max} (excitation)) ≤ 0.1): λ_{max} (emission) = 595, 676 (two forms were observable) nm (Figure S61). UV−vis (PBS/DMSO, 99:1, v/v, c ∼ 1.1×10^{-5} mol dm^{-3}): λ_{max} = 664, 619, 401, 328 nm (Figure 2c). Fluorescence (PBS/DMSO, 99:1, v/v, A (λ_{max} (excitation)) ≤ 0.1): λ_{max} (emission) = 606, 682 nm (Figure 2c). HRMS (APCI$^+$−TOF) m/z: $[M + H]^+$ calcd for $C_{31}H_{43}N_6O_6Si$ 623.3008; found 623.3012. pK_a (nonbuffered aqueous solution, I = 0.1 mol dm^{-3}) = 6.76 ± 0.11.

Note: A mixture of two regioisomers in the ratio of ∼55:45 was obtained and clearly distinguished by NMR; two anomers of the saccharide were also distinguished in the NMR spectra (Figure S59).

*N-(3,7-Bis(dimethylamino)-5,5-dimethyldibenzo[b,e]silin-10(5H)-ylidene)-2-(1-((4R,5S,6R)-2,4,5-trihydroxy-6-(hydroxymethyl)-tetrahydro-2H-pyran-3-yl)-1H-1,2,3-triazol-4-yl)ethanesulfonamide (**2g**).* This compound was synthesized from **2e** and 2-azido-2-deoxy-D-glucose. Yield: 29 mg (86%). Orange crystalline solid. Mp: 123.5−128.5

°C. ^{1}H NMR (500 MHz, $CDCl_3$): δ (ppm) 0.47 (s, 6H, >Si(CH_3)$_2$), 3.10 (s, 12H, −N(CH_3)$_2$), 3.41−3.52 (m, 1.9H), 3.55−3.60 (m, 2.4H), 3.71−3.79 (m, 1.3H), 3.64 (d, 0.6H, J = 2.6 Hz), 3.82−3.94 (m, 1.7H), 4.06−4.10 (m, 1H), 4.23 (t, 0.7H, J = 9.7 Hz), 4.57 (d, 0.3H, J = 2.6 Hz), 4.59 (d, 0.3H, J = 2.6 Hz), 5.08 (d, 0.5H, J = 7.1 Hz) 5.26 (d, 0.6H, J = 2.8 Hz), 6.81 (d, 2H, J = 8.8 Hz), 6.94 (br s, 2H), 7.86 (s, 0.45H, =N−C(CH_2)=C*H*−N(glu)−, regioisomer b), 7.97 (s, 0.55H, =N−C(CH_2)=C*H*−N(glu)−, regioisomer a), 8.21 (d, 2H, J = 8.7 Hz) (Figure S65). ^{13}C NMR (126 MHz, $CDCl_3$): δ (ppm) −1.8 (>Si(CH_3)$_2$), 40.1 (−N(CH_3)$_2$), 56.4, 56.5 (both −CH_2−), 62.6, 62.7 (both −CH_2−), 67.0, 69.8, 71.8, 72.1, 72.5, 73.3, 75.6, 78.2, 92.7 (glu: −CH(OH)−O−, anomer 1), 96.2 (glu: −CH(OH)−O−, anomer 2), 113.3 (C_{ar}H), 116.1 (C_{ar}H), 123.8 (=N−C(CH_2)=CH−N(glu)−, regioisomer a, only observed in ^{1}H−^{13}C HSQC), 125.5 (, =N−C(CH_2)=CH−N(glu)−, regioisomer b) 130.6 ($C_{ar(q)}$), 134.0 (C_{ar}H), 141.2 ($C_{ar(q)}$), 153.1 ($C_{ar(q)}$), 176.4 (>*C*=N−SO_2−) (Figure S66). MS (EI): m/z = 645 (M^+, not visible), 460 (<1), 429 (1), 369 (4), 323 (40), 308 (29), 295 (12), 281 (8), 221 (13), 194 (8), 168 (14), 148 (19), 110 (24), 97 (33), 84 (100), 55 (46). FTIR (cm^{-1}): 3295, 2925, 2109, 1581, 1363, 1253, 1062, 1019, 956, 839, 762. UV−vis (CH_3OH, $c = 4.3 \times 10^{-5}$ mol dm^{-3}): λ_{max} (log ε) = 218 (4.32), 245 (4.13), 391 (4.10), 447 (4.18) nm (dm^3 mol^{-1} cm^{-1}) (Figure S67). Fluorescence (CH_3OH, A (λ_{max} (excitation)) ≤ 0.1): λ_{max} (emission) = 616 nm (Figure S67). UV−vis (PBS/DMSO, 99:1, v/v, $c = 2.7 \times 10^{-5}$ mol dm^{-3}): λ_{max} = 469, 404, 246 nm (dm^3 mol^{-1} cm^{-1}) (Figure 3). Fluorescence (PBS/DMSO, 99:1, v/v, A (λ_{max} (excitation)) ≤ 0.1): λ_{max} (emission) = 631 nm (Figure 3). HRMS (ESI$^+$−TOF) m/z: [M + H]$^+$ calcd for $C_{29}H_{41}N_6O_7SSi$ 645.2521; found 645.2525. pK_a (nonbuffered aqueous solution, I = 0.1 mol dm^{-3}) ~ 2.7 ± 0.7.

Note: A mixture of two regioisomers in the ratio of ~55:45 was obtained and clearly distinguished by NMR; two anomers of the saccharide were also distinguished in the NMR spectra (Figure S64).

■ ASSOCIATED CONTENT

Supporting Information

Photophysical properties of selected fluorophores, NMR, IR, Raman, UV/vis, fluorescence spectra, quantum chemical calculations data, and stability determination experiments. This material is available free of charge via the Internet at http://pubs.acs.org.

■ AUTHOR INFORMATION

Corresponding Author

* E-mail: klan@sci.muni.cz. Phone: +420-54949-4856. Fax: +420-54949-2443.

Notes

The authors declare no competing financial interest.

■ ACKNOWLEDGMENTS

Support for this work was provided by the Grant Agency of the Czech Republic (13-25775S), the Czech Ministry of Education (LO1214) (P.K.), and the project "Employment of Best Young Scientists for International Cooperation Empowerment" (CZ.1.07/2.3.00/30.0037) cofinanced from the European Social Fund and the state budget of the Czech Republic (P.Š.). P.H. was supported by the AXA Fund. The authors express their thanks to Lukáš Maier, Miroslava Bittová, Lubomír Prokeš and Zdeněk Moravec for their help with the NMR measurements, and mass and Raman spectrometry. Ján Krausko is acknowledged for his help with the fluorescence measurements, and Jakob Wirz and Lukáš Maier for fruitful discussions. We thank Tomáš Pastierik for his help with synthesis of some precursors. The computational facilities of University of Fribourg are acknowledged for the computational resources.

■ REFERENCES

(1) Wysocki, L. M.; Lavis, L. D. *Curr. Opin. Chem. Biol.* **2011**, *15*, 752.
(2) Ueno, T.; Nagano, T. *Nat. Methods* **2011**, *8*, 642.
(3) Gonçalves, M. S. T. *Chem. Rev.* **2009**, *109*, 190.
(4) Lavis, L. D.; Raines, R. T. *ACS Chem. Biol.* **2008**, *3*, 142.
(5) Lavis, L. D.; Raines, R. T. *ACS Chem. Biol.* **2014**, *9*, 855.
(6) Takaoka, Y.; Ojida, A.; Hamachi, I. *Angew. Chem., Int. Ed.* **2013**, *52*, 4088.
(7) Weissleder, R.; Ntziachristos, V. *Nat. Med.* **2003**, *9*, 123.
(8) Frangioni, J. V. *Curr. Opin. Chem. Biol.* **2003**, *7*, 626.
(9) Lakowicz, J. R. *Principles of Fluorescence Microscopy*; Springer: New York, 2006.
(10) Escobedo, J. O.; Rusin, O.; Lim, S.; Strongin, R. M. *Curr. Opin. Chem. Biol.* **2010**, *14*, 64.
(11) Nienhaus, K.; Ulrich Nienhaus, G. *Chem. Soc. Rev.* **2014**, *43*, 1088.
(12) Zems, Y.; Moiseev, A. G.; Perepichka, D. F. *Org. Lett.* **2013**, *15*, 5330.
(13) Zhu, C.; Li, S.; Luo, M.; Zhou, X.; Niu, Y.; Lin, M.; Zhu, J.; Cao, Z.; Lu, X.; Wen, T.; Xie, Z.; Schleyer, P. v. R.; Xia, H. *Nat. Chem.* **2013**, *5*, 698.
(14) Wang, F.; Tan, W. B.; Zhang, Y.; Fan, X. P.; Wang, M. Q. *Nanotechnology* **2006**, *17*, R1.
(15) Mertz, E. L.; Tikhomirov, V. A.; Krishtalik, L. I. *J. Phys. Chem. A* **1997**, *101*, 3433.
(16) Klan, P.; Wirz, J. *Photochemistry of organic compounds: From concepts to practice*, 1st ed.; John Wiley & Sons Ltd.: Chichester, 2009.
(17) Liang, H. C.; Zhang, C. X.; Henson, M. J.; Sommer, R. D.; Hatwell, K. R.; Kaderli, S.; Zuberbuhler, A. D.; Rheingold, A. L.; Solomon, E. I.; Karlin, K. D. *J. Am. Chem. Soc.* **2002**, *124*, 4170.
(18) Liu, X. G.; Xu, Z. C.; Cole, J. M. *J. Phys. Chem. C* **2013**, *117*, 16584.
(19) Fan, J. L.; Hu, M. M.; Zhan, P.; Peng, X. J. *Chem. Soc. Rev.* **2013**, *42*, 29.
(20) Wu, L.; Burgess, K. *Org. Lett.* **2008**, *10*, 1779.
(21) Lee, B.-Y.; Park, S. R.; Jeon, H. B.; Kim, K. S. *Tetrahedron Lett.* **2006**, *47*, 5105.
(22) Pastierik, T.; Šebej, P.; Medalová, J.; Štacko, P.; Klán, P. *J. Org. Chem.* **2014**, *79*, 3374.
(23) Berezin, M. Y.; Achilefu, S. *Chem. Rev.* **2010**, *110*, 2641.
(24) Valdesaguilera, O.; Neckers, D. C. *J. Phys. Chem.* **1988**, *92*, 4286.
(25) Antonov, L.; Gergov, G.; Petrov, V.; Kubista, M.; Nygren, J. *Talanta* **1999**, *49*, 99.
(26) We need to note here that the errors of the estimates of vertical transition energies for absorption and fluorescence, which we computed by the TD-PBE0 functional, do not vary systematically and depend on the character of the substituent in the position 9 of the dye (Table 3). Several other functionals (B3LYP, BMK, CAM-B3LYP, M06, and M06-2X) have been tested but provided similar or even lower quality results. The DFT methods seem to underestimate the vertical excitation energies for the dyes that have a formal exo double bond on C9, while they overestimate the excitation energies when a single bond between C9 and N is present. This can be nicely demonstrated by comparing the absorption and emission properties of the two acid−base forms (A and B) of **1a** with those of **5** and **7a**, respectively. We decided to inspect the behavior of various DFT methods for a larger set of related pyronin molecules, which is, however, beyond the scope of the current work, and it will be presented in a forthcoming study. The computed Stokes shifts are, nevertheless, in semiquantitative agreement with the experimental values, and allow for at least qualitative description of the factors that govern the large observed Stokes shifts.
(27) Santoro, F.; Improta, R.; Lami, A.; Bloino, J.; Barone, V. *J. Chem. Phys.* **2007**, 126.
(28) Koide, Y.; Urano, Y.; Hanaoka, K.; Terai, T.; Nagano, T. *ACS Chem. Biol.* **2011**, *6*, 600.
(29) Egawa, T.; Koide, Y.; Hanaoka, K.; Komatsu, T.; Terai, T.; Nagano, T. *Chem. Commun.* **2011**, *47*, 4162.
(30) Urano, Y.; Kamiya, M.; Kanda, K.; Ueno, T.; Hirose, K.; Nagano, T. *J. Am. Chem. Soc.* **2005**, *127*, 4888.
(31) Beija, M.; Afonso, C. A. M.; Martinho, J. M. G. *Chem. Soc. Rev.* **2009**, *38*, 2410.

(32) Fu, M.; Xiao, Y.; Qian, X.; Zhao, D.; Xu, Y. *Chem. Commun.* **2008**, 1780.
(33) Burgess, K., US Pat. 2009/0192298.
(34) Zilles, A.; Drexhage, K. H.; Kemnitzer, N. U.; Arden-Jacob, J.; Hamers-Schneider, M. WO Pat. 2012/052435.
(35) Ritchie, C. D.; Kubisty, C.; Ting, G. Y. *J. Am. Chem. Soc.* **1983**, *105*, 279.
(36) Ray, P. C.; Sen, D. C. *J. Indian Chem. Soc.* **1930**, *7*, 275.
(37) Sugawara, S.; Kojima, S.; Yamamoto, Y. *Chem. Commun.* **2012**, *48*, 9735.
(38) Hymel, D.; Woydziak, Z. R.; Peterson, B. R. *J. Am. Chem. Soc.* **2014**, *136*, 5241.
(39) Allen, F. H.; Kennard, O.; Watson, D. G.; Brammer, L.; Orpen, A. G.; Taylor, R. *J. Chem. Soc., Perkin Trans. 2* **1987**, S1.
(40) Stokes shifts are mostly presented in the wavelength scale, which is convenient for imaging applications, but inappropriate in discussions about their physical origin. Therefore, we report the values of Stokes shifts in both wavelengths (in nm) and wavenumbers.
(41) Bremberg, U.; Ringberg, E.; Berts, W.; de Belder, A.; Strickland, J. S. US Pat. 2013/0096309 A1.
(42) Marek, R.; Lycka, A. *Curr. Org. Chem.* **2002**, *6*, 35.
(43) Savarin, C. G.; Boice, G. N.; Murry, J. A.; Corley, E.; DiMichele, L.; Hughes, D. *Org. Lett.* **2006**, *8*, 3903.
(44) Attanasi, O. A.; De Crescentini, L.; Filippone, P.; Giorgi, G.; Mantellini, F.; Mazzanti, A. *Synlett* **2006**, 2403.
(45) Grabowski, Z. R.; Rotkiewicz, K.; Rettig, W. *Chem. Rev.* **2003**, *103*, 3899.
(46) Shaikh, M.; Mohanty, J.; Singh, P. K.; Bhasikuttan, A. C.; Rajule, R. N.; Satam, V. S.; Bendre, S. R.; Kanetkar, V. R.; Pal, H. *J. Phys. Chem. A* **2010**, *114*, 4507.
(47) Soujanya, T.; Fessenden, R. W.; Samanta, A. *J. Phys. Chem.* **1996**, *100*, 3507.
(48) Zhao, G. J.; Han, K. L. *Acc. Chem. Res.* **2012**, *45*, 404.
(49) Alvarez-Pez, J. M.; Ballesteros, L.; Talavera, E.; Yguerabide, J. *J. Phys. Chem. A* **2001**, *105*, 6320.
(50) Martinez-Peragon, A.; Miguel, D.; Jurado, R.; Justicia, J.; Alvarez-Pez, J. M.; Cuerva, J. M.; Crovetto, L. *Chem.—Eur. J.* **2014**, *20*, 447.
(51) Orte, A.; Crovetto, L.; Talavera, E. M.; Boens, N.; Alvarez-Pez, J. M. *J. Phys. Chem. A* **2005**, *109*, 734.
(52) Wallrabe, H.; Periasamy, A. *Curr. Opin. Biotechnol.* **2005**, *16*, 19.
(53) Benniston, A. C.; Harriman, A.; Lawrie, D. J.; Mayeux, A. *Phys. Chem. Chem. Phys.* **2004**, *6*, 51.
(54) Peng, X. J.; Song, F. L.; Lu, E.; Wang, Y. N.; Zhou, W.; Fan, J. L.; Gao, Y. L. *J. Am. Chem. Soc.* **2005**, *127*, 4170.
(55) Kaneda, K.; Arai, T. *Photochem. Photobiol. Sci.* **2003**, *2*, 402.
(56) Morgenthaler, M. J. E.; Yoshihara, K.; Meech, S. R. *J. Chem. Soc., Faraday Trans.* **1996**, *92*, 629.
(57) Titus, J. A.; Haugland, R.; Sharrow, S. O.; Segal, D. M. *J. Immunol. Methods* **1982**, *50*, 193.
(58) Sjoback, R.; Nygren, J.; Kubista, M. *Spectrochim. Acta, Part A* **1995**, *51*, L7.
(59) Siejak, P.; Frackowiak, D. *J. Chem. Phys. B* **2005**, *109*, 14382.
(60) Taniguchi, T.; Wang, J.; Irle, S.; Yamaguchi, S. *Dalton T.* **2013**, *42*, 620.
(61) ATTO-Tec GmbH, Fluorescent Labels and Dyes, Product Catalogue 2013/2015, Siegen, Germany.
(62) Sanguineti, A.; Sassi, M.; Turrisi, R.; Ruffo, R.; Vaccaro, G.; Meinardi, F.; Beverina, L. *Chem. Commun.* **2013**, *49*, 1618.
(63) Schill, H.; Nizamov, S.; Bottanelli, F.; Bierwagen, J.; Belov, V. N.; Hell, S. W. *Chem.—Eur. J.* **2013**, *19*, 16556.
(64) Yang, Y. J.; Lowry, M.; Xu, X. Y.; Escobedo, J. O.; Sibrian-Vazcluez, M.; Wong, L.; Schowalter, C. M.; Jensen, T. J.; Fronczek, F. R.; Warner, I. M.; Strongin, R. M. *Proc. Nat. Acad. Sci. U.S.A.* **2008**, *105*, 8829.
(65) Sletten, E. M.; Bertozzi, C. R. *Angew. Chem., Int. Ed.* **2009**, *48*, 6974.
(66) Han, J. Y.; Burgess, K. *Chem. Rev.* **2010**, *110*, 2709.
(67) Gottlieb, H. E.; Kotlyar, V.; Nudelman, A. *J. Org. Chem.* **1997**, *62*, 7512.
(68) Olah, G. A.; Kiovsky, T. E. *J. Am. Chem. Soc.* **1968**, *90*, 4666.
(69) Frisch, M. J.; Trucks, G. W.; Schlegel, H. B.; Scuseria, G. E.; Robb, M. A.; Cheeseman, J. R.; Scalmani, G.; Barone, V.; Mennucci, B.; Petersson, G. A.; Nakatsuji, H.; Caricato, M.; Li, X.; Hratchian, H. P.; Izmaylov, A. F.; Bloino, J.; Zheng, G.; Sonnenberg, J. L.; Hada, M.; Ehara, M.; Toyota, K.; Fukuda, R.; Hasegawa, J.; Ishida, M.; Nakajima, T.; Honda, Y.; Kitao, O.; Nakai, H.; Vreven, T.; Montgomery, J. A., Jr.; Peralta, J. E.; Ogliaro, F.; Bearpark, M.; Heyd, J. J.; Brothers, E.; ; Kudin, K. N.; Staroverov, V. N.; Kobayashi, R.; Normand, J.; Raghavachari, K.; Rendell, A.; Burant, J. C.; Iyengar, S. S.; Tomasi, J.; Cossi, M.; Rega, N.; Millam, J. M.; Klene, M.; Knox, J. E.; Cross, J. B.; Bakken, V.; Adamo, C.; Jaramillo, J.; Gomperts, R.; Stratmann, R. E.; Yazyev, O.; Austin, A. J.; Cammi, R.; Pomelli, C.; Ochterski, J. W.; Martin, R. L.; Morokuma, K.; Zakrzewski, V. G.; Voth, G. A.; Salvador, P.; Dannenberg, J. J.; Dapprich, S.; Daniels, A. D.; Farkas, Ö.; Foresman, J. B.; Ortiz, J. V.; Cioslowski, J.; Fox, D. J.; Gaussian, Inc.,: Wallingford, CT, 2009.
(70) Adamo, C.; Barone, V. *J. Chem. Phys.* **1999**, *110*, 6158.
(71) Jacquemin, D.; Planchat, A.; Adamo, C.; Mennucci, B. *J. Chem. Theory Comput.* **2012**, *8*, 2359.
(72) Jin, J. L.; Li, H. B.; Geng, Y.; Wu, Y.; Duan, Y. A.; Su, Z. M. *ChemPhysChem* **2012**, *13*, 3714.
(73) Earl, R. A.; Vollhardt, K. P. C. *J. Org. Chem.* **1984**, *49*, 4786.
(74) Kolb, R.; Bach, N. C.; Sieber, S. A. *Chem. Commun.* **2014**, *50*, 427.
(75) Chanteau, S. H.; Tour, J. M. *J. Org. Chem.* **2003**, *68*, 8750.
(76) Cheung, F. K.; Hayes, A. M.; Morris, D. J.; Wills, M. *Org. Biomol. Chem.* **2007**, *5*, 1093.
(77) Stacko, P.; Sebej, P.; Veetil, A. T.; Klan, P. *Org. Lett.* **2012**, *14*, 4918.